MID-AMERICA TRANSPORTATION CENTER

Report # MATC-UNL: 004-12

Final Report
WBS: 25-1121-0005-004-12

Investigation and Development of a Test Level 6 Barrier Phase II

Jennifer Rasmussen, PhD, P.E.
Research Assistant Professor
Midwest Roadside Safety Facility
Department of Civil and Environmental Engineering
University of Nebraska-Lincoln

Cody S. Stolle, PhD
Research Assistant Professor
Department of Mechanical and Materials Engineering

Ronald K. Faller, PhD, P.E.
Research Professor
Department of Civil and Environmental Engineering

Joshua S. Steelman, PhD, P.E.
Assistant Professor
Department of Civil and Environmental Engineering

Elisa Vasquez, B.S.M.E.
Graduate Research Assistant
Department of Mechanical and Materials Engineering

Seok Hwan Yoo, B.S.C.E.
Graduate Research Assistant
Department of Civil and Environmental Engineering

2020

A Cooperative Research Project sponsored by
U.S. Department of Transportation- Office of the Assistant Secretary for Research and Technology

Investigation and Development of a MASH Test Level 6 Barrier, Phase II
Draft Report

Jennifer Rasmussen, Ph.D., P.E. (PI)
Research Assistant Professor
Midwest Roadside Safety Facility
Department of Civil and Environmental Engineering
University of Nebraska-Lincoln

Cody S. Stolle, Ph.D.
Research Assistant Professor
Midwest Roadside Safety Facility
Department of Mechanical and Materials Engineering
University of Nebraska-Lincoln

Ronald K. Faller, Ph.D., P.E. (Co-PI)
Research Professor
Midwest Roadside Safety Facility
Department of Civil and Environmental Engineering
University of Nebraska-Lincoln

Joshua S. Steelman, PhD., P.E. (Co-PI)
Assistant Professor
Department of Civil and Environmental Engineering
University of Nebraska-Lincoln

Elisa Vasquez, B.S.M.E.
Graduate Research Assistant
Department of Mechanical and Materials Engineering
University of Nebraska-Lincoln

Seok Hwan Yoo, B.S.C.E.
Graduate Research Assistant
Department of Civil and Environmental Engineering
University of Nebraska-Lincoln

A Report on Research Sponsored by

Mid-America Transportation Center

University of Nebraska–Lincoln

January 2020

INVESTIGATION AND DEVELOPMENT OF A MASH TEST LEVEL 6 BARRIER, PHASE II

Submitted by

Elisa Vasquez, B.S.M.E.
Graduate Research Assistant

Seok Hwan Yoo, B.S.C.E.
Graduate Research Assistant

Cody S. Stolle, PhD.
Research Assistant Professor

Jennifer D. Rasmussen, Ph.D., P.E.
Research Assistant Professor

Ronald K. Faller, Ph.D., P.E.
Research Professor and MwRSF Director

Joshua S. Steelman, Ph.D., P.E.
Assistant Professor

MIDWEST ROADSIDE SAFETY FACILITY
Nebraska Transportation Center
University of Nebraska-Lincoln
130 Whittier Research Center
2200 Vine Street
Lincoln, Nebraska 68583-0853
(402) 472-0965

Submitted to

MID-AMERICA TRANSPORTATION CENTER
2200 Vine Street
Lincoln, Nebraska 68583

MwRSF Research Report No. TRP-03-430-20

January 2020

TECHNICAL REPORT DOCUMENTATION PAGE

<table>
<tr><td>1. Report No.
25-1121-0005-004-12</td><td colspan="2">2. Government Accession No.</td><td colspan="2">3. Recipient's Accession No.</td></tr>
<tr><td colspan="3" rowspan="2">4. Title and Subtitle
Investigation and Development of a Test Level 6 Barrier, Phase II</td><td colspan="2">5. Report Date
January 2020</td></tr>
<tr><td colspan="2">6. Performing Organization Code</td></tr>
<tr><td colspan="3">7. Author(s)
Jennifer Rasmussen, PhD ORCID: 0000-0003-0909-0850
Cody S. Stolle, PhD ORCID: 0000-0001-6674-7383
Ronald K. Faller, PhD ORCID: 0000-0001-7660-1572
Joshua S. Steelman, PhD ORCID: 0000-0002-8664-7520
Elisa Vasquez, B.S.M.E.
Seok Hwan Yoo, B.S.C.E.</td><td colspan="2">8. Performing Organization Report No.
25-1121-0005-004-12</td></tr>
<tr><td colspan="3" rowspan="2">9. Performing Organization Name and Address
Midwest Roadside Safety Facility (MwRSF)
Nebraska Transportation Center
University of Nebraska-Lincoln
130 Whittier Research Center
2200 Vine Street
Lincoln, Nebraska 68583-0853</td><td colspan="2">10. Project/Task/Work Unit No.</td></tr>
<tr><td colspan="2">11. Contract or Grant (G) No.
69A3551747107</td></tr>
<tr><td colspan="3" rowspan="2">12. Sponsoring Organization Name and Address
Mid-America Transportation Center
2200 Vine St
PO Box 830851
Lincoln, NE 68583</td><td colspan="2">13. Type of Report and Period Covered
Final Report: 2019-2020</td></tr>
<tr><td colspan="2">14. Sponsoring Agency Code
MATC TRB RiP No. 91994-32</td></tr>
<tr><td colspan="5">15. Supplementary Notes
Conducted in cooperation with U.S. Department of Transportation, Federal Highway Administration.</td></tr>
<tr><td colspan="5">16. Abstract
The objective of this research project was to develop and analyze a new, cost-effective, MASH TL-6 barrier which would contain a tractor-tank trailer vehicle. To evaluate barrier designs, it was first necessary to develop a validated tank-trailer model which could be towed by a tractor vehicle. This research report describes the development of the tank trailer.
A literature review was conducted which evaluated different computational methods to simulate fluid inside a tank. Using geometry of the BKZ 5949 gasoline/oil/fuel tank provided by the LBT Inc., located in Omaha, Nebraska, MwRSF researchers generated a tank, suspension, and fluid model. The model was simulated in static and dynamic configurations and was attached to a pre-existing model of a tractor.
Four viable fluid modeling techniques were considered and models of each fluid were implemented into the tank model. The weights of the fluids were calculated based on the empty static weights of the tractor and trailer.</td></tr>
<tr><td colspan="3">17. Document Analysis/Descriptors
Highway Safety, MASH, Test Level 6, Roadside Barrier, LS-DYNA, Tractor-Tank Trailer, Fluid Modeling</td><td colspan="2">18. Availability Statement
No restrictions. Document available from: National Technical Information Services, Springfield, Virginia 22161</td></tr>
<tr><td>19. Security Class (this report)
Unclassified</td><td>20. Security Class (this page)
Unclassified</td><td>21. No. of Pages
68</td><td colspan="2">22. Price</td></tr>
</table>

Table of Contents

List of Figures

List of Tables

Acknowledgements

The authors wish to acknowledge several sources that made a contribution to this project: (1) the Mid-America Transportation Center; (2) LBT Inc. for providing information on tank trailers; and (3) the Holland Computing Center at the University of Nebraska, which receives support from the Nebraska Research Initiative.

Acknowledgement is also given to the following individuals who made a contribution to the completion of this research project.

Midwest Roadside Safety Facility

J.C. Holloway, M.S.C.E., E.I.T., Assistant Director –Physical Testing Division
K.A. Lechtenberg, M.S.M.E., E.I.T., Research Engineer
R.W. Bielenberg, M.S.M.E., E.I.T., Research Engineer
S.K. Rosenbaugh, M.S.C.E., E.I.T., Research Engineer
C.S. Stolle, Ph.D., Research Assistant Professor
M. Asadollahi Pajouh, Ph.D., Research Assistant Professor
A.T. Russell, B.S.B.A., Testing and Maintenance Technician II
E.W. Krier, B.S., Construction and Testing Technician II
S.M. Tighe, Construction and Testing Technician I
D.S. Charroin, Construction and Testing Technician I
Z. Jabr, Construction and Testing Technician I
R.M. Novak, Construction and Testing Technician I
J.E. Kohtz, B.S.M.E., CAD Technician
E.L. Urbank, B.A., Research Communication Specialist
Undergraduate and Graduate Research Assistants

Abstract

The objective of this research project was to develop and analyze a new, cost-effective, MASH TL-6 barrier which would contain a tractor-tank trailer vehicle. To evaluate barrier designs, it was first necessary to develop a validated tank-trailer model which could be towed by a tractor vehicle. This research report describes the development of the tank trailer.

A literature review was conducted which evaluated different computational methods to simulate fluid inside a tank. Using geometry of the BKZ 5949 gasoline/oil/fuel tank provided by the LBT Inc., located in Omaha, Nebraska, MwRSF researchers generated a tank, suspension, and fluid model. The model was simulated in static and dynamic configurations and was attached to a pre-existing model of a tractor.

Four viable fluid modeling techniques were considered and models of each fluid were implemented into the tank model. The weights of the fluids were calculated based on the empty static weights of the tractor and trailer.

Disclaimer Statement

The contents of this report reflect the views of the authors, who are responsible for the facts and the accuracy of the information presented herein. This document is disseminated in the interest of information exchange. The report is funded, partially or entirely, by a grant from the U.S. Department of Transportation's University Transportation Centers Program. However, the U.S. Government assumes no liability for the contents or use thereof.

Chapter 1 Introduction

1.1 Background

Roadside and median barriers, including bridge rails, have been commonly used to prevent run-off-road (ROR) events, and to prevent errant motorists from striking hazardous fixed objects or geometric features, thus mitigating the severity of those crashes. For the ROR situations, it is deemed appropriate to utilize barrier systems that are capable to safely contain and redirect passenger vehicles. These barriers typically meet the Test Level 3 (TL-3) safety performance guidelines published in either the National Cooperative Highway Research Program (NCHRP) report No. 350, *Recommended Procedures for the Safety Performance Evaluation of Highway Features* [1] or the American Association of State highway and Transportation Officials (AASHTOs) *Manual for Assessing Safety Hardware* [2]. A TL-3 test condition utilizes two type of vehicle, a 2,420-lb (1,100-kg) passenger car and a 5,000-lb (2,270-kg) pick-up truck, to impact the barrier at a speed of 62 mph (100 km/h) at a 25 degree angle.

However, there are situations in which it may be necessary to use higher-performance vehicle containment barriers (i.e., TL-4 through TL-6) when the percentage of truck and other heavy vehicle traffic is high and/or the consequences of vehicle penetration beyond the longitudinal barrier is too great. TL-4, TL-5, and TL-6 test vehicles are a 22,000-lb (10,000-kg) single unit truck, 80,000-lb (36,000-kg) tractor-van trailer truck, and a 80,000-lb (36,000-kg) tractor-tank trailer truck, respectively TL-4, TL-5, and TL-6 impact conditions are 56 mph (90 km/h) at 15 degrees, 50 mph (80 km/h) at 15 degrees, and 50 mph (80 km/h) at 15 degrees respectively.

To date, only one Test Level 6 vehicle containment system was successfully tested and evaluated according to NCHRP Report 230 [3] safety performance criteria using a tractor tank trailer vehicle. This combination barrier system consisted of a lower reinforced concrete solid

parapet with an upper beam and post railing system and measured 90 in. tall. Unfortunately, the cost, height, and appearance of this TL-6 containment barrier have prevented its widespread implementation. Due to its current configuration and cost, few TL-6 barriers have been utilized in the real-world thus far. These situations could include prevention and mitigation of: (1) cross median, opposing-traffic, vehicle crashes involving hazardous heavy tanker trucks along urban freeways and interstates and (2) tanker vehicle penetration or override of existing TL-4 or TL-5 barriers located on bridges, elevated road structures, or high volume roadways, which create potential catastrophic events near schools, malls, sports venues, concert arenas, military bases, international airports, critical government buildings, or other high-risk facilities. As such, there exists a need to develop, a new, cost-effective, structurally adequate, reduced-height, vehicle containment system that is safe for motorists, is capable of containing errant vehicle impacts with heavy tanker-truck vehicles, and prevents and/or mitigates the consequences of catastrophic crashes into high-risk facilities or highly-populated areas.

1.2 Objective

The objective of this project was to develop a new, cost-effective, *Manual for Assessing Safety Hardware* (MASH) Test Level 6 (TL-6) barrier [2]. This barrier should be able to safely redirect vehicles ranging from 2,420-lb (1,100-kg) small passenger cars to 80,000-lb (36,000kg) tractor-tank trailers. The new barrier designs were developed on Phase I of this project. In order to validate the results of the new TL-6 barrier, computer simulation programs as LS-DYNA was developed and will be used to evaluate barrier strengths and impact loads. The objective of this research effort was to closely model the geometry and performance of the fluid-filled tank using realistic part geometries, and model and implement fluid into the tank.

1.3 Research Scope

The objective will be achieved through the completion of several tasks. First, a literature review was completed describing techniques for modeling fluids and fluid-container interactions using finite element analysis. Various fluid modeling techniques were identified and parameters associated with those models were archived. Next, researchers utilized the tank geometry of the elliptical straight-frame 5949 trailer produced by LBT Inc to generate a finite element mesh using finite element analysis preprocessors HyperMesh and LS PrePost. The part geometries were extracted from computer-aided drafting (CAD) files and SolidWorks, and the material properties were taken from reference guides, research papers, and LBT specifications. Component constraints were added to the model to mimic fasteners such as bolts and nuts. Contacts were also added to allow the tank to impact external features, as well as to allow tank components to interact with each other during dynamic events. Different techniques were employed to generate fluid meshes to reside within the interior tank structure. Preliminary properties for the fluids were generated using reference materials from published papers. Finally, the tank structure was connected to the truck at a 5^{th} wheel pin connection using rigid nodal constraints. Alternative concrete properties for the barrier model were also explored.

1.4 Primary Units

The majority of the research described in this research report was completed using the finite element analysis (FEA) software LS-DYNA. For consistency in the simulations, all simulations, geometries, and quantities described in models were completed using metric units and with base mass, distance, and time units of kg, mm, and ms, respectively. Therefore, in this report, metric units are considered standard and are typically reported in quantities which are conducive for LS-DYNA use. Common metric unit representations using the base kg-mm-ms units are shown in table 1.1.

Table 1.1 Common Metric Units

Parameter	Base Unit	Unit Conversion
Mass	kg	-
Distance	mm	-
Time	ms	-
Acceleration	g	$\mathrm{g's} = \dfrac{acceleration\ \left(\frac{\mathrm{mm}}{\mathrm{ms}^2}\right)}{earth\ gravity = \ 0.00981\ \frac{\mathrm{mm}}{\mathrm{ms}^2}}$
Force	kN	$1\ \mathrm{kN} \equiv 1\ \mathrm{kg}\left(1\frac{\mathrm{mm}}{\mathrm{ms}^2}\right)$
Energy	J	$1\ \mathrm{J} \equiv 1\ \mathrm{kg}\left(1\frac{\mathrm{mm}}{\mathrm{ms}^2}\right) * 1\ \mathrm{mm}$
Volume	L	$1\ \mathrm{L} = 1{,}000\ \mathrm{mL}$ $1\ \mathrm{mL} = 1\ \mathrm{mm}^3$

Chapter 2 Literature Review

2.1 Scope of Review

When a truck-tank-trailer run-off-road event occurs, these accidents are associated to be a dangerous situation. These vehicles carry hazardous liquid contents such as chemicals, gasoline, and fuel oils; therefore the containment and stability of tank vehicles is important. One of the main concerns is the fluid sloshing behavior in filled or partially filled containers, which may dynamically load against the side of a tank and create vehicle and trailer instability. Slosh refers to the periodic movement of a liquid inside of a container, in this case the oscillatory motion of the liquid inside the tank structures. For this reason, the literature review was primarily focused on the Fluid Structure Interaction (FSI) inside the tank for stable tank-trailer interactions during dynamic impact events.

The cited research reports relevant to fluid slosh were reviewed to formulate the current knowledge and status for fluid modeling analysis. The reviewed reports are briefly summarized below, particularly focused on: (i) tank design standards to focus on limitations of current design concerning on the effect of fluid sloshing; (ii) methods of analysis of liquid slosh in moving containers; and (iii) vehicle simulation.

2.2 Review of tank design

The majority of roadside safety design is focused on the safety of occupants of passenger vehicles and may also include consideration for the containment of large trucks. The American Association of State Highway and Transportation Officials (AASHTO) published the *Manual for Assessing Safety Hardware* (MASH) which was revised in 2016 [2]. When appropriate to evaluate large truck impacts, three test vehicle designations may be utilized: a 22,000-lb (10,000-kg) single-unit truck (SUT) for TL-4; an 80,000-lb (36,000-kg) tractor trailer vehicle for TL-5; and an 80,000-lb (36,000-kg) tractor-tank trailer vehicle for TL-6. Representative vehicles used

in tests conducted according to MASH test levels TL-4, TL-5, and TL-6 are shown in Figures figures 2.1 and 2.2.

Figure 2.1 TL-4 (top), TL-5 (middle), and TL-6 (bottom) vehicles

Figure 2.2 MASH Test Vehicle Back End Geometries: TL-4 (left), TL-5 (middle), and TL-6 (right)

2.3 Liquid sloshing

The problem of fluid sloshing motion inside a spherical or cylindrical tank, which is usually described by three dimensional flow [7], has been studied since the 1960's. The liquid sloshing influences the safety performance of tank-trailer vehicles because of the hydrodynamic forces and moments created from the liquid oscillation inside the tank, thus reducing the stability of the filled or partially filled tank vehicle. Tank-trailer vehicles have anti-slosh devices, known as "baffles", which reduces the motion of the liquid and provides stability to the tank vehicle. Numerical, and FEA has been performed to optimize the safety performance of tank-trailer vehicles, mostly focusing on the analyzation of the sloshing behavior inside the tank in order to come up with new techniques in fuel tanks to reduce these phenomena.

2.4 Computational Fluid Dynamic Method in LS-DYNA

For more than 50 years the problem of sloshing was investigated, improving the accuracy on the analysis. FEA has significantly improved the Fluid Structure Interaction (FSI) modelling

techniques. These techniques have been utilized to investigate the behavior of fluids due to the variation of fluid flow and pressure during an impact, and the complexity of water when flasked inside a tank. There are different methods of modeling fluid; advantages and limitations from each method will be discussed.

2.4.1 Lagrangian Formulation

The computational mesh of Lagrangian formulation is usually used for describing and analyzing the behavior of deformable structures, but for some fluid problems, a Lagrangian mesh may provide a reasonable fluid behavior. In Lagrangian formulation nodes are connected to each other with a material medium and the mesh is attached to material and therefore the mesh follows the fluid material. If the fluid material experiences a large distortion it will lead an increase in time processing or analysis termination [8]. For this formulation, the interaction between the fluid and structure is modeled using a contact in which the fluid is defined as a slave. Because the fluid material is continuous and utilizes discrete and deterministic surfaces defined by the user, only a single fluid mass can be modeled (no mixing). Fluid cavitation or intra-fluid transitions, such as fluid waves breaking against the side of the tank, cannot be modeled because the elements must remain continuous and in the same nodal orders and cannot self-intersect.

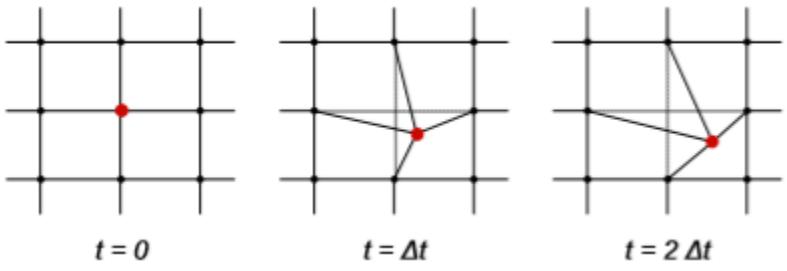

Figure 2.3 Lagrangian Mesh Deformations

2.4.2 Eulerian formulation

The Eulerian formulation for fluid flow analysis advances solutions in time on a mesh fixed on space. The Eulerian method avoids the Lagrangian problem of mesh distortion by fixing nodes in space and calculating future discrete time steps at each iteration for computational efficiency [8]. As a result, the Eulerian method allows mass flow between elements. The Eulerian method consist of a Lagrangian computation at every time step, followed by a re-map phase which restores the distorted mesh to its original state. A disadvantage of the Eulerian approach is that a fine mesh is required to capture the material response, this makes the method computationally expensive.

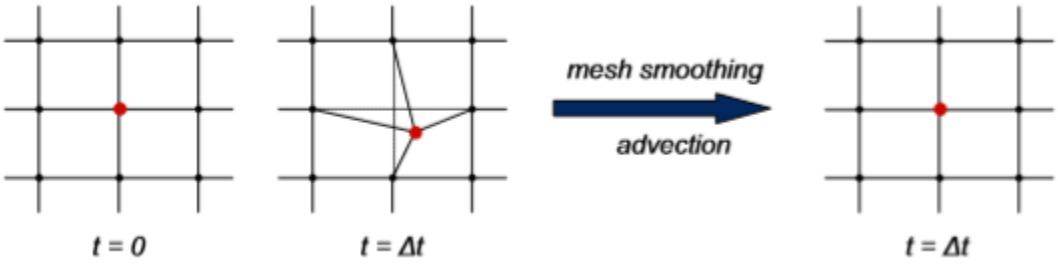

Figure 2.4 Pure Eulerian

2.4.3 Arbitrary Lagrangian-Eulerian (ALE) formulation

The computational ALE is a finite element formulation created by combining features of Lagrangian and Eulerian computational methods [9]. The Lagrangian domain evaluates the movement and/or deformation of structural components of the model and allows mass flow between elements, as well as fluid surface deformations and surface tension calculations. The Eulerian domain deals with the movement of the air or fluid. The motion of the mesh is independent of the motion of the analyzed material. The advantage of the ALE computational

method is that allows smoothing of a distorted mesh without performing a complete re-mesh. However, ALE methods require careful consideration for contacts, material definition, and flow.

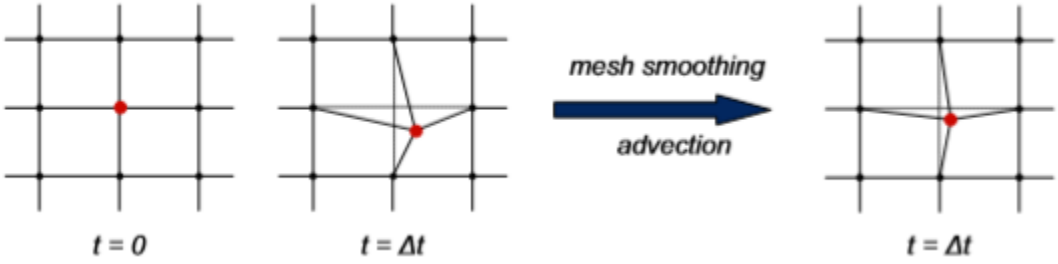

Figure 2.5 Arbitrary Lagrangian-Eulerian

2.4.4 Soothed Particle Hydrodynamics (SPH)

SPH is a meshless Lagrangian method, it does not suffer from mesh distortion in large deformation problems [9]. Models comprised of SPH definitions evaluate the movement of packets of material, evaluated as smooth spherical particles, which can interact with each other with surface-to-surface contacts, Van der Waals forces, mixing friction, and tensile or compressive forces. Each SPH element remains rigid and spherical throughout the simulation. Because the computation requires the computation of inter-particle dynamics and kinematics of many particles and a fine mesh is often required to accurately model fluid behaviors, SPH methods tend to be computationally expensive.

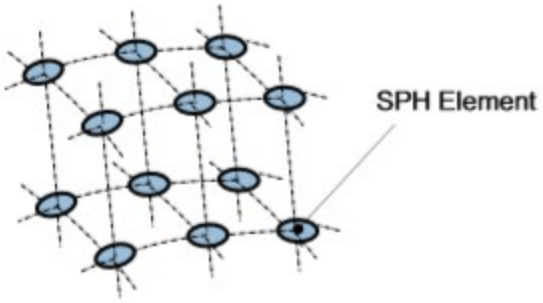

Figure 2.6 Smooth Particle Hydrodynamics

2.4.5 Discrete Element Spheres (DES)

Another discrete particle method, similar to SPH, is the use of discrete element spheres (DES). The DES method is a recent development and is supported in versions of LS-DYNA starting with 9.71 [12]. DES modeling allows users to define friction break angles, surface friction and roughness, densities, and inertias per element. Each element consists of a rigid discrete sphere but has volumetric size which is independently defined. As a result, DES formulations can use a combination of multiple particle sizes to represent different granular distributions and packing efficiencies. While DES was intended to model granular materials and media, with a large number of particles, continuous media (such as fluids) may be reasonable in some applications. The DES method is shown schematically in figure 2.7.

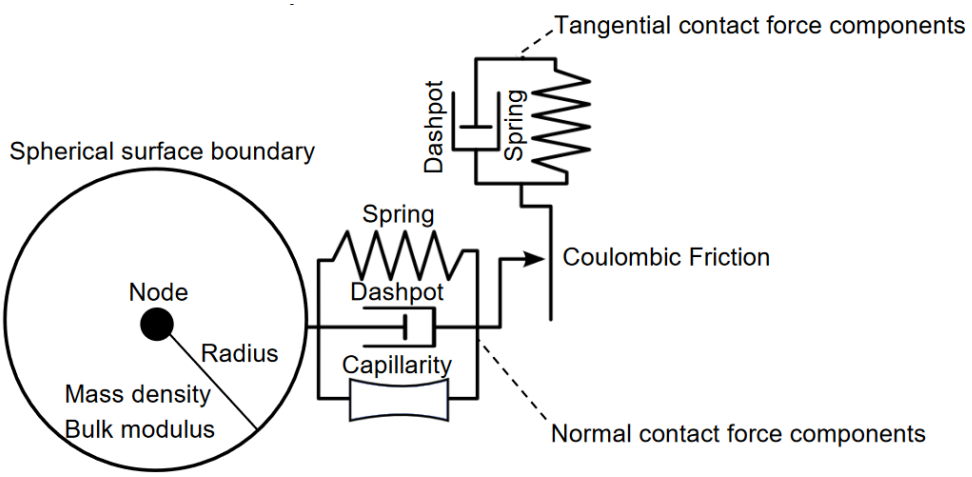

Figure 2.7 Contact Definition for DES Elements [12]

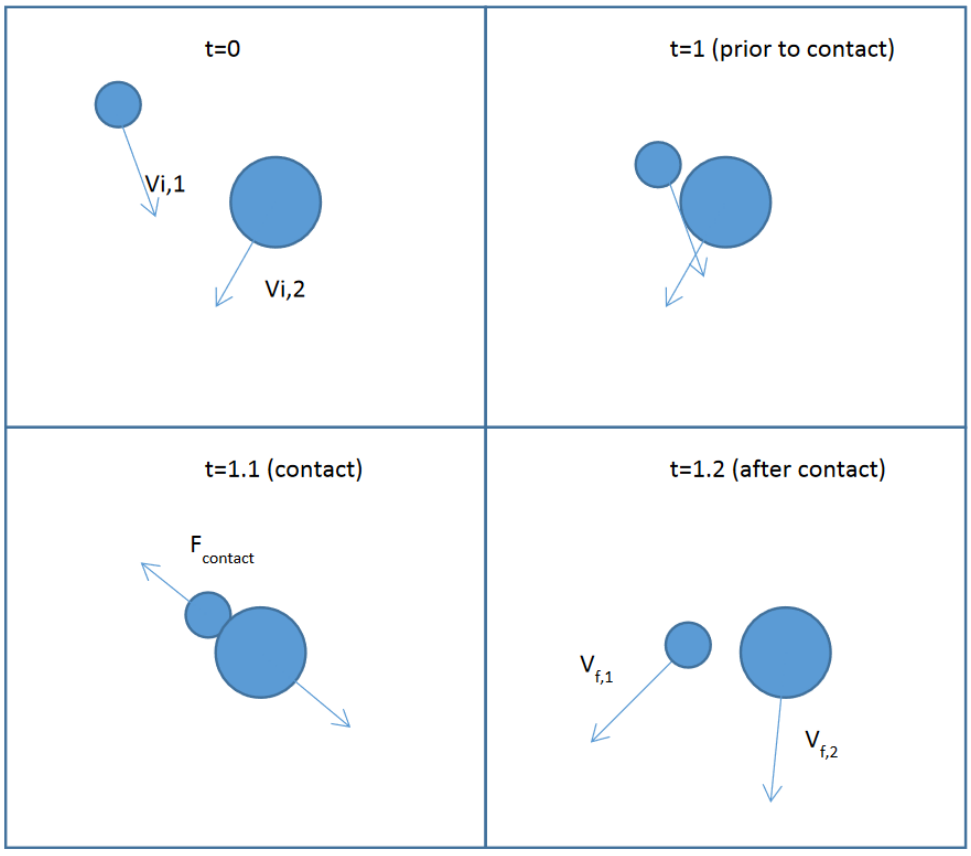

Figure 2.8 Schematic of DES Impact Dynamics [13]

2.5 Summary of Fluid Modeling Techniques

The considerations, including advantages and disadvantages of each fluid model, were compared. The analysis of fluid modeling techniques is shown in table 2.1. Due to similarity with SPH methods in terms of material interactions, contact, and model behavior, SPH and DES methods are lumped for consideration. Note that comparisons are subjective and may differ based on how techniques are applied in different models. Moreover, challenging FSI interactions may require additional considerations than those shown.

Table 2.1 Summary and Comparison of FSI Computational Methods

	Computational Method			
	Lagrangian	**Eulerian**	**ALE**	**SPH**
Applications	Structure interaction and describing solid mechanics problems	Fluid-structure analysis	Fluid-structure analysis	Fluid-structure interaction, splashing and sloshing
Type of Element	single material	single material or multi material	single material or multi material	Single material
Mesh	Yes	Yes	Yes	No
Re-meshing	In Lagrangian mesh is not re-zoned to their original position	In Eulerian formulation the nodes are re-zoned to their original positions	Mesh is either not re-zonde (Lagrangian) and re-zoned to it's original shape (Eulerian)	No need for re-meshing
Computational Time	Low computational time	High computational time, time step remains constant	High computational time, Lagrangian motion is computed every timestep	Low computational time
Model Requirements	Each part need to be assigned to a material or constitutive model	Refined mesh for accuracy, define void elements where material may flow	One material per mesh, nodes within the mesh	Initial desnity needs to be specified, equation of state needs to be assigned
Advantages	Free surface is followed automatically	Avoids mesh distortion, efficient for large element deformations	Meshing is quicker to set-up, elements can be integral with the Lagrangian structure, use traditional contact methods.	No mesh distortion in large deformation problems
General Limitations	Mesh distortion and lose accuracy in large deformation problems	Limitations in modelling interfaces	Element distortion	Consistency issues, tensile instability and zero energy modes

Chapter 3 Deformable Concrete Barrier Modeling using Existing TL-5 Vehicle

3.1 Introduction

In the Year 1 study of this project, the TL-6 truck model impacted the Concept 3 Modified Design, which incorporated a rigid concrete barrier and deformable steel posts and rails [4]. The truck model was believed to be underpredicting loads, and it was recommended to develop a new truck model. It was also desired to model the concrete more realistically, instead of as a rigid material. Thus, the rigid concrete barriers were replaced by deformable concrete barriers with steel reinforcement, while the rest of the barrier model remained the same. This effort occurred concurrently with the development of the new truck model and utilized the existing truck model to explore materials only. The purpose of applying the realistic reinforced concrete material property to the model was to observe the change in the performance of the barrier model in terms of the exerted force and damage to the barrier. The existing TL-6 truck model impacted the barrier model at 50 mph and 15 degrees. The angular displacement and change in velocity of the TL-6 vehicle model were also compared to the baseline model utilizing rigid concrete elements.

3.2 Deformable TL-6 Barrier Model

The reinforced concrete parapet was comprised of ten 10-ft long parapets with a total system length of 100 ft, as shown in figure 3.1. The 10-ft long parapets were continuous but were separate parts to track forces along the length of the system barrier. The model consisted of reinforced concrete barriers, steel rails, posts, base plates, reinforcements, anchorage bolts, and foundation. In order to represent the realistic behavior of barriers under the dynamic impact, each component was developed by using input parameters tested by previous researchers.

The constitutive concrete model was MAT_CSCM_CONCRETE material model, which is a smooth continuous surface cap model developed and validated by the Federal Highway

Administration to predict the dynamic behaviors of the concrete in roadside safety hardware under vehicle collision. The CSCM model can be utilized in two options, one of which autogenerates the parameter based on the limited number of inputs, and the other option requires all input parameters. Initially, the material properties were autogenerated by inputting the concrete strength and the maximum size of aggregates, which were 5,000 psi (0.035 GPa) and ¾ in. (19 mm), respectively. The concrete component of the barrier was generated by using eight-node constant stress solid brick elements. The concrete barrier cross-section was 18 in. wide and 42 in. tall, as shown in figure 3.1. The mesh size of the concrete barrier was 1-in. cube, for a total of 907,200 solid elements. The material properties for the deformable barriers, steel posts, and steel reinforcement are shown in table 3.1.

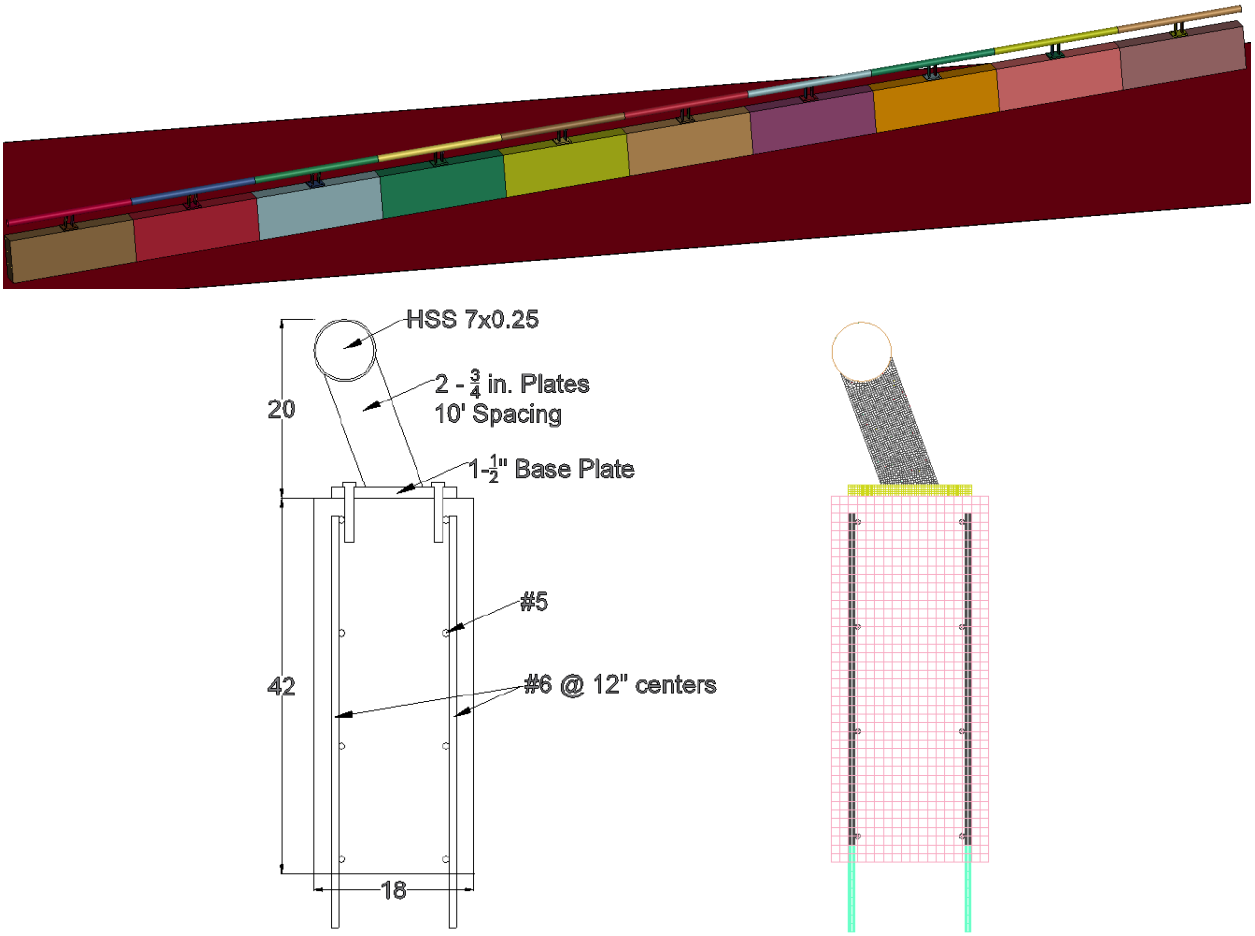

Figure 3.1 Modified concept 3 drawing and LS-DYNA model

Table 3.1 List of simulation parts and LS-DYNA Parameters

Part Name	Element Type	Element Formulation	Material Type	Material Formulation
Concrete Barrier	Solid	Constant Stress	5,000 psi Concrete	CSCM Concrete
Steel Post	Solid	Constant Stress	ASTM A992 Steel	Piecewise Linear Plasticity
Base Plate	Solid	Constant Stress	ASTM A992 Steel	Piecewise Linear Plasticity
Reinforcement	Beam	Hughes-Liu	ASTM A615 Gr. 60	Piecewise Linear Plasticity
Steel Rail	Shell	Belytschko-Tsay	ASTM A500 Grade B	Piecewise Linear Plasticity

The steel reinforcement was generated by using the Hughes-Liu beam element and embedded into the concrete barriers. The material properties were applied to the MAT_ PIECEWISE_LINEAR_PLASTICITY keyword, and the inputs were summarized in table 3.2. For the vertical reinforcements, no. 6 rebars were selected and placed 12 in. apart. The clear cover was 2-in. from the concrete surface. Four longitudinal no. 5 rebars were placed on each of the traffic-side and back-side surfaces. The top and bottom longitudinal rebars were 3 in. from the top and the bottom surfaces of the concrete barrier. The CONSTRAINED_BEAM_IN_SOLID keyword was used to establish a bond between the rebars and barriers. This command constrains the slave beam elements to move with solid elements, which serve as the master components.

The steel base plates needed to be constrained to the concrete either with an explicitly modeled anchor or another connection. To simplify the connection initially, the nodes on the bottom of the base plate bolt holes and nodes on the top of the concrete barrier near the bolt holes were constrained using the CONSTRAINED_NODAL_RIGID_BODIES keyword. This

command is commonly used to define a rigid connection between structural parts. No failure can occur in the nodal rigid bodies between the base plate and the concrete barriers.

Table 3.2 Input parameters for steel reinforcement

Parameters	Values	Units
Density	7.86E-06	Kg/mm3
Young's Modulus	200	GPa
Yield Strength	0.46	GPa
Poisson's Ratio	0.28	N/A

In order to simulate the bonding between the concrete barrier and the foundation, all of the nodes at the bottom of the barrier were fixed in all motions using the BOUNDARY_SPC keyword. Constraining the bottom barrier nodes was the simplest way to replicate the fixed conditions, but unrealistic element erosion occurred at the base of the concrete barriers, as shown below. The bottom elements were undamaged when the front axle and the tandem-axle of the truck impacted, but several bottom elements on the traffic-side eroded when the rear-axle impacted, as shown in figure 3.2.

The concrete barrier remained intact, even though more than half of the elements at the bottom deleted. This behavior seemed unrealistic. Thus, a foundation was considered to more realistically model the ground line fixity. The foundation design from a previous MASH TL-5 barrier was utilized initially, as shown in figure 3.3 [5]. The width and height of the foundation were 900 mm and 600 mm, respectively, and they were converted to the nearest inch, 36 in. and 24 in., in the LS-DYNA model. 20M bars were used for the foundation reinforcements, and they were converted to no. 5 rebars. The spacing between the stirrups was 300 mm in the drawing, and it was converted to 12 in. in order to align the reinforcement in the same spacing to the

vertical reinforcements. No. 5 rebar at 12 in. spacing connected the concrete barrier and the foundation. Anchorages were embedded 8 in. into the foundation and 16 in. into the barrier. The deformable barrier, along with a concrete foundation and reinforcement, is shown in figure 3.4. The same material property used for the concrete barrier was applied to the foundation, and the same material property used for the concrete barrier reinforcement was applied to the reinforcement embedded in the foundation. The concrete foundation and the reinforcement were constrained by using the CONSTRAINED_BEAM_IN_SOLID keyword, which was also used within the concrete barrier.

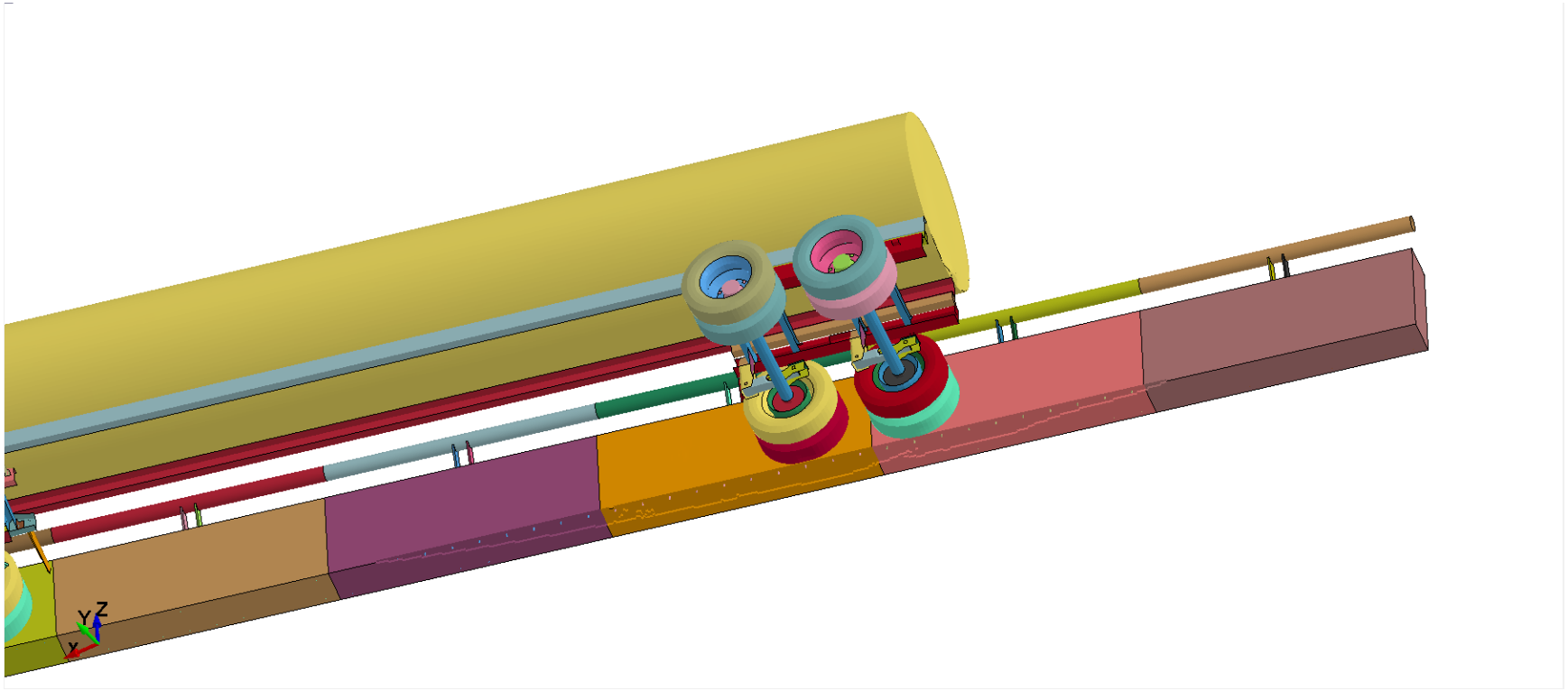

Figure 3.2 Element erosion due to impact by the rear-axle

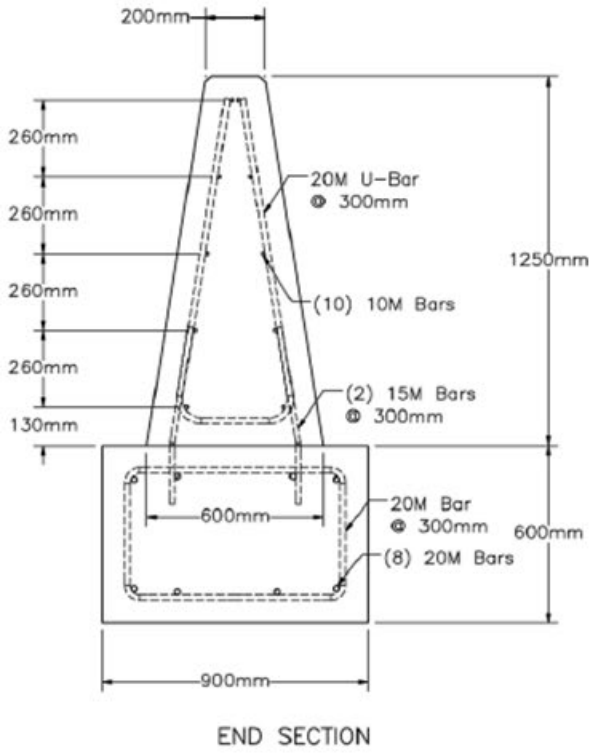

Figure 3.3 Previous TL-5 foundation design layout for median barriers [5]

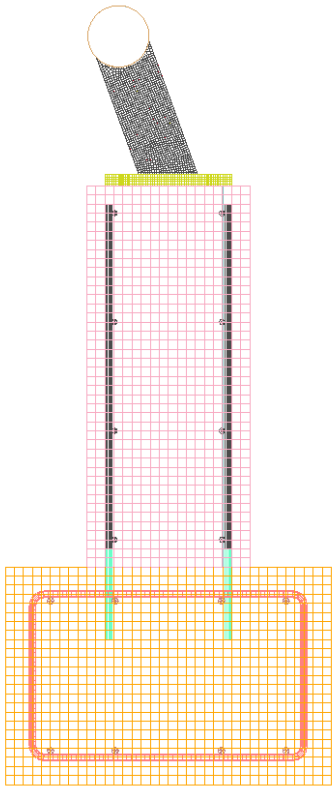

Figure 3.4 Modified concept 3 barrier with a foundation

3.3 Simulation Result of TL-6 Model

A TL-6 tank-trailer truck model impacted the concrete parapet with foundation at a speed of 50 mph and at an angle of 15 degrees. The initial impact in the simulation occurred 27.5 ft downstream from the upstream end of the barrier. The simulation results were evaluated based on the MASH 2016 evaluation criteria A, D, and G, which were summarized in table 3.3. Sequential images of the simulation are shown in figure 3.5.

Table 3.3 MASH 2016 Evaluation Criteria

MASH 2016 Criteria	
Criteria A	The test article should contain and redirect the vehicle or bring the vehicle to a controlled stop; the vehicle should not penetrate, underride, or override the installation although controlled lateral deflection of the test article is acceptable
Criteria D	Detached elements, fragments, or other debris from the test article should not penetrate, or show potential for penetrating the occupant compartment
Criteria G	the vehicle remains upright during and after collision

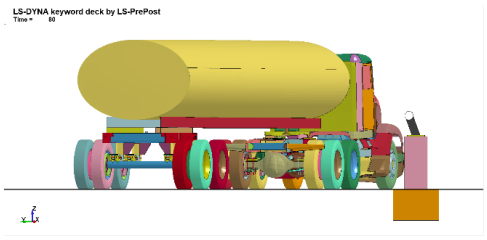

0 msec

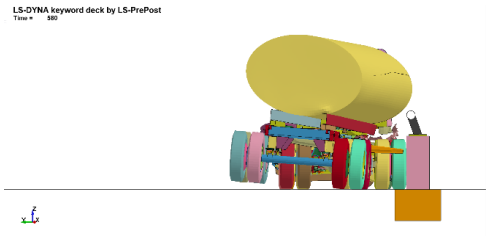

500 msec

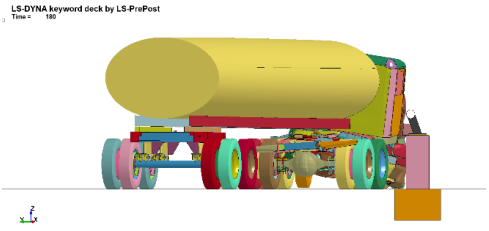

100 msec

600 msec

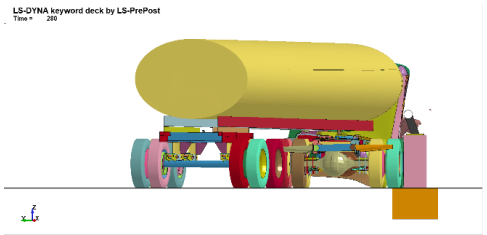

200 msec

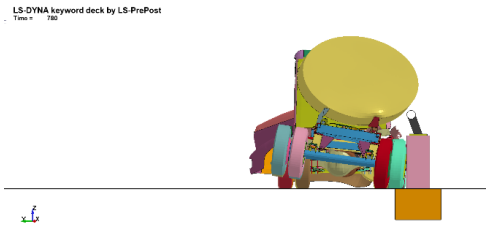

700 msec

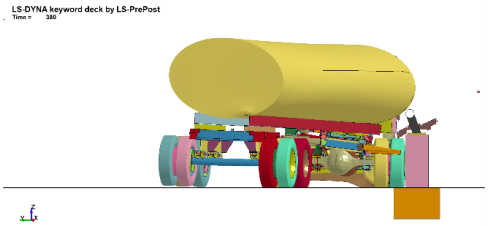

300 msec

800 msec

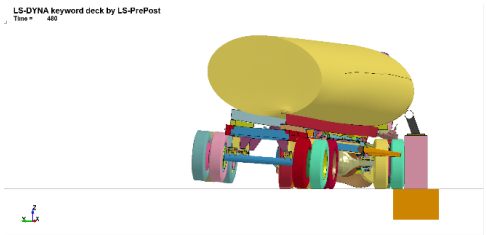

400 msec

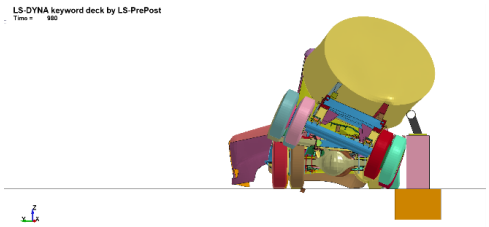

900 msec

Figure 3.5 Simulation Sequential

3.3.1 Barrier Damage

The damage to the barrier model was minimal. Barrier nos. 7, 8, and 9 are shown in figure 3.6, which were considered to be subjected to most of the damage due to the impact. Element erosion, visible dynamic deflection, and permanent deflection were not observed on the surface during the simulation. The von mises stress plots were created for the impacts of the front wheel, tandem axle, and rear axle on the concrete barrier. The stress plot ranged from 0 GPa to 0.034 GPa, which were 0 ksi to 5 ksi, as shown in figure 3.7. Tire marks were visible along the front face of the barrier nos. 7 to 9 in the simulation. The connection between the concrete barrier and the base plate remained intact during the vehicle collision. The stress level on the surface was approximately 2 ksi, which represents that the stress was below the specified compressive strength of the concrete material model.

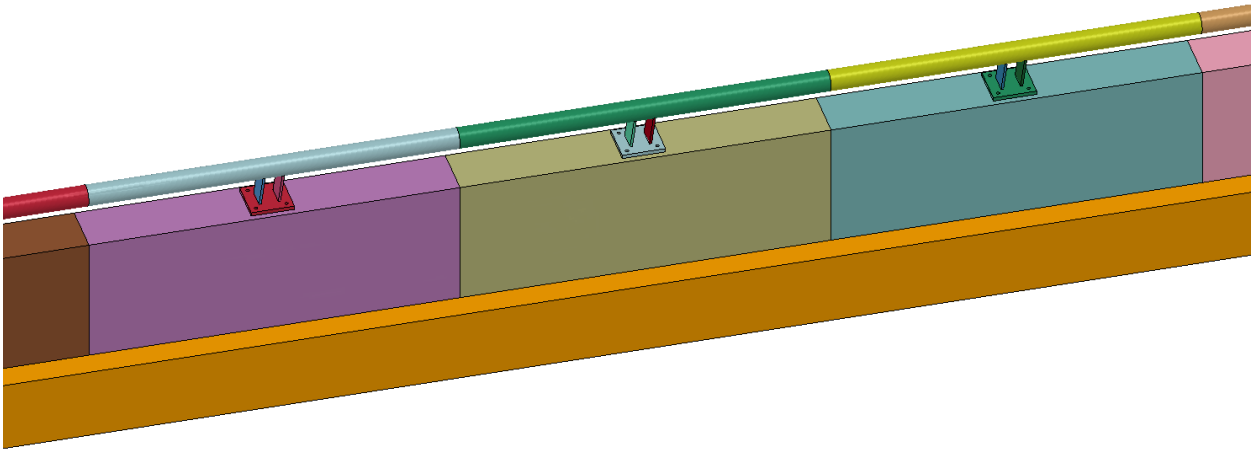

Figure 3.6 Barrier nos 7, 8, and 9 after the impact

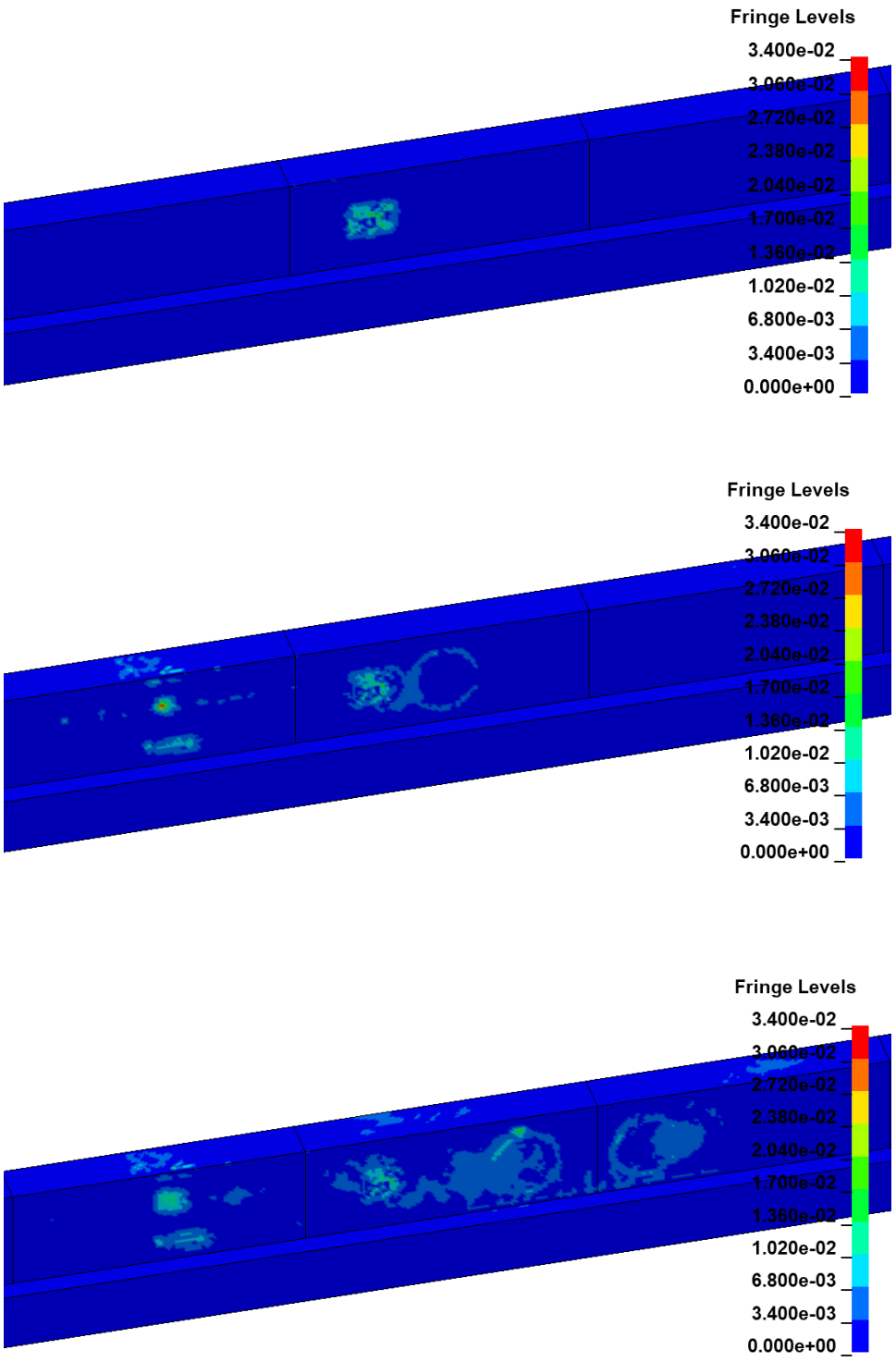

Figure 3.7 Von mises stress contour plot on barrier nos 7, 8, and 9 at 40 msec, 220 msec, and 620 msec

The damage on the steel rail was minimal, as shown in figure 2.8 and figure 3.9. Steel rails were not detached from the steel posts, and tear-out on the steel rail was not observed. The dents were found on the steel rail nos. 4 and 7 during the simulation, which was caused by the roll of the trailer when the rear-axle of the trailer impacted the barrier. The maximum resultant displacement on the steel rail no. 4 was 19 mm and the maximum resultant displacement on the steel rail no. 7 was 9 mm.

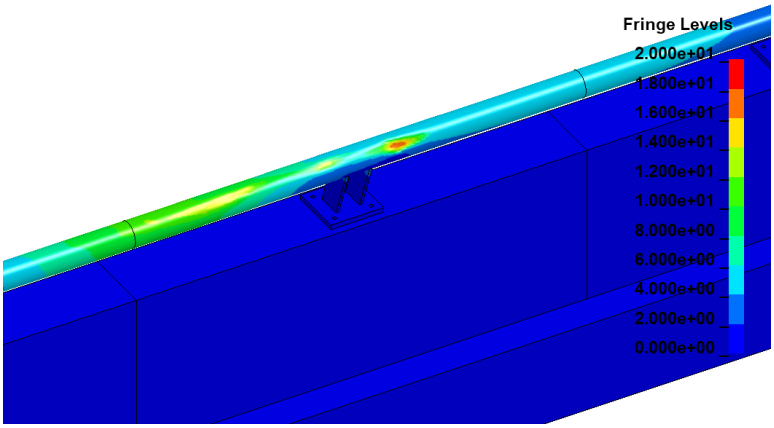

Figure 3.8 Resultant displacement on the steel rail no. 4

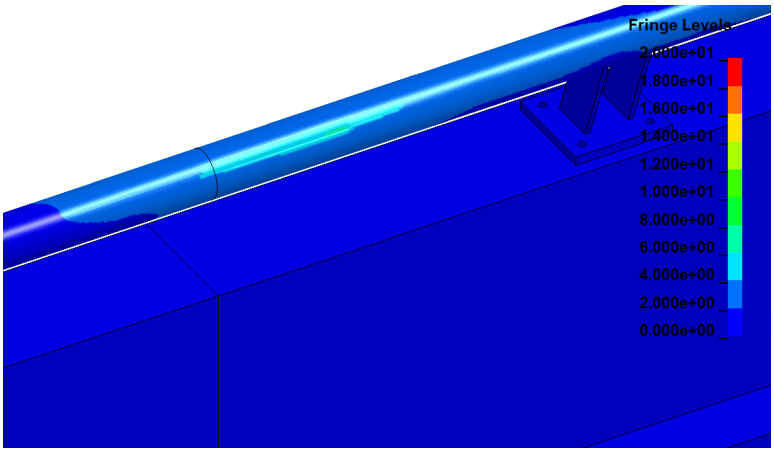

Figure 3.9 Resultant displacement on the steel rail no. 7

3.3.2 Force Comparison

Contact forces were measured between the vehicle and the barrier. The forces applied by the TL-6 vehicle model to the previous rigid concrete barrier baseline model, along with a total load, are shown in figure 3.10 [4]. Three distinctive peaks occurred, which were caused by the impact of the front-axle, the tandem-axle, and the rear-axle. The force and time plot for the deformable barrier system is shown in figure 3.11. The exerted force on the barrier was expected to be lower than the baseline model because the deformable barrier absorbs some of the kinetic energy from the impact. The forces in the x-axis and y-axis exerted by concrete barriers and steel rails were collected at a frequency of 10,000 Hz. The force data were processed by using the Butterworth filter with a cutoff frequency of 100 Hz and 50 msec moving average. The recorded force in the deformable barrier model was smaller than the baseline model, but the contribution of the steel rail in terms of containing the impact force was also lower as compared to the baseline model. The difference in terms of exerted force on the two systems was compared and is shown in table 3.4.

3.3.3 Angular Displacement Comparison

The baseline rigid barrier model and the deformable barrier model angular displacement of the rear-axle is shown in figure 3.12 [4] and figure 3.13, respectively. The change in angular displacement was not significant. The rear-axle in the deformable barrier rolled 3.4 degrees, 12 percent, less than that of the rigid barrier simulation, and the yaw and pitch decreased by 1.6 and 0.5 degrees, respectively. The lower angular displacement represented that the truck model had increased stability compared to that of the rigid barrier, as shown in table 3.5.

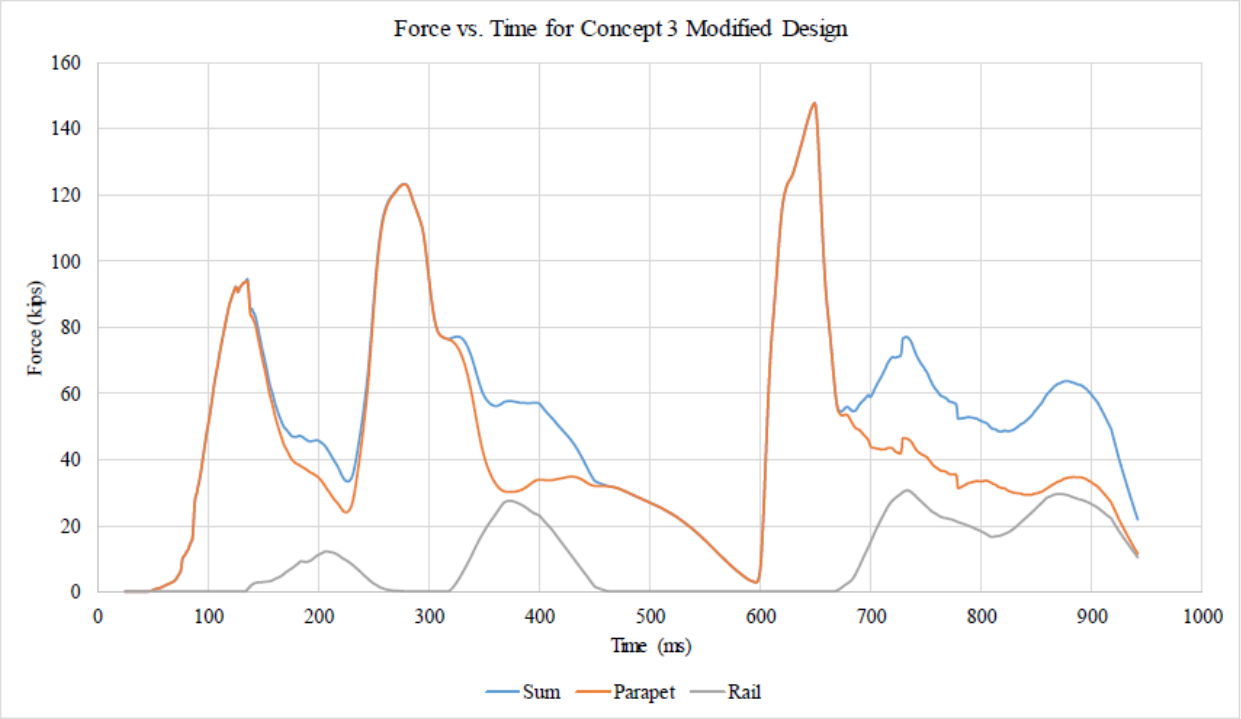

Figure 3.10 Force vs. Time plot for the rigid barriers [4]

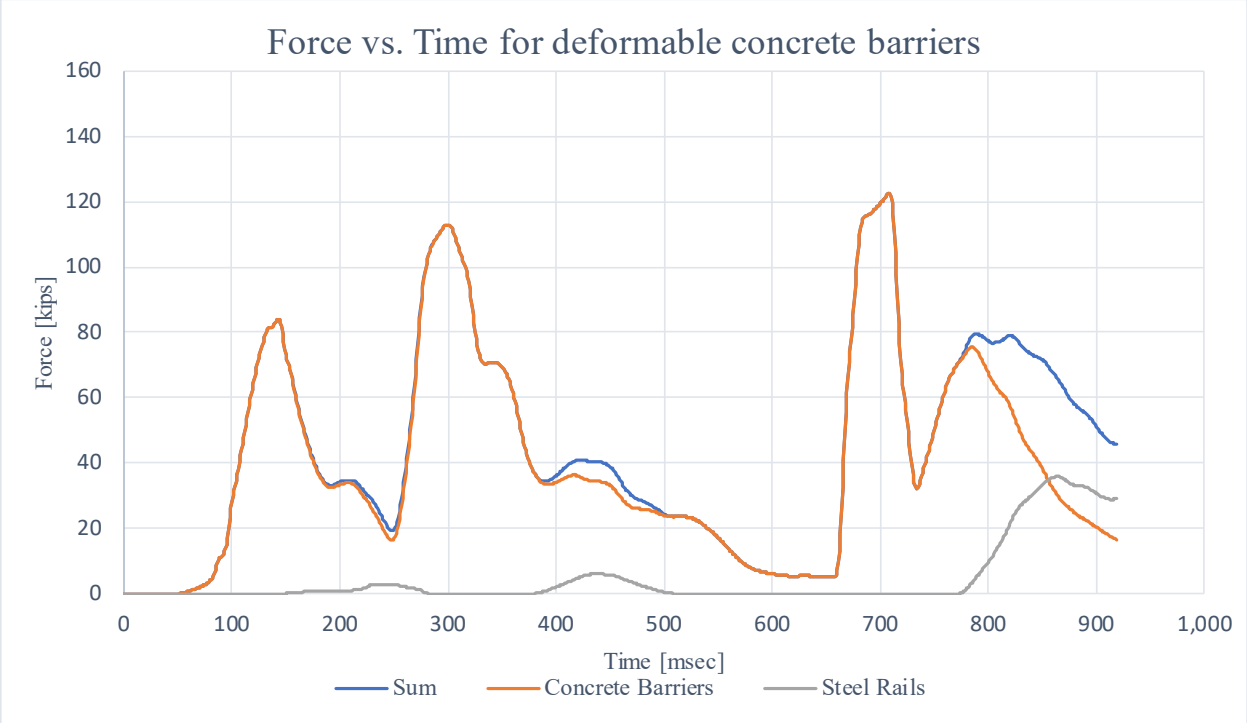

Figure 3.11 Force vs. Time plot for the deformable barrier

Table 3.4 Peak forces on the rigid barrier and the deformable barrier

Parameter	Rigid Simulation Force	Deformable Simulation Force	Deformable Difference Compared to Rigid
First peak force	95 kips	83 kips	13% lower
Second Peak force	122 kips	111 kips	9% lower
Third Peak force	147 kips	124 kips	16% lower

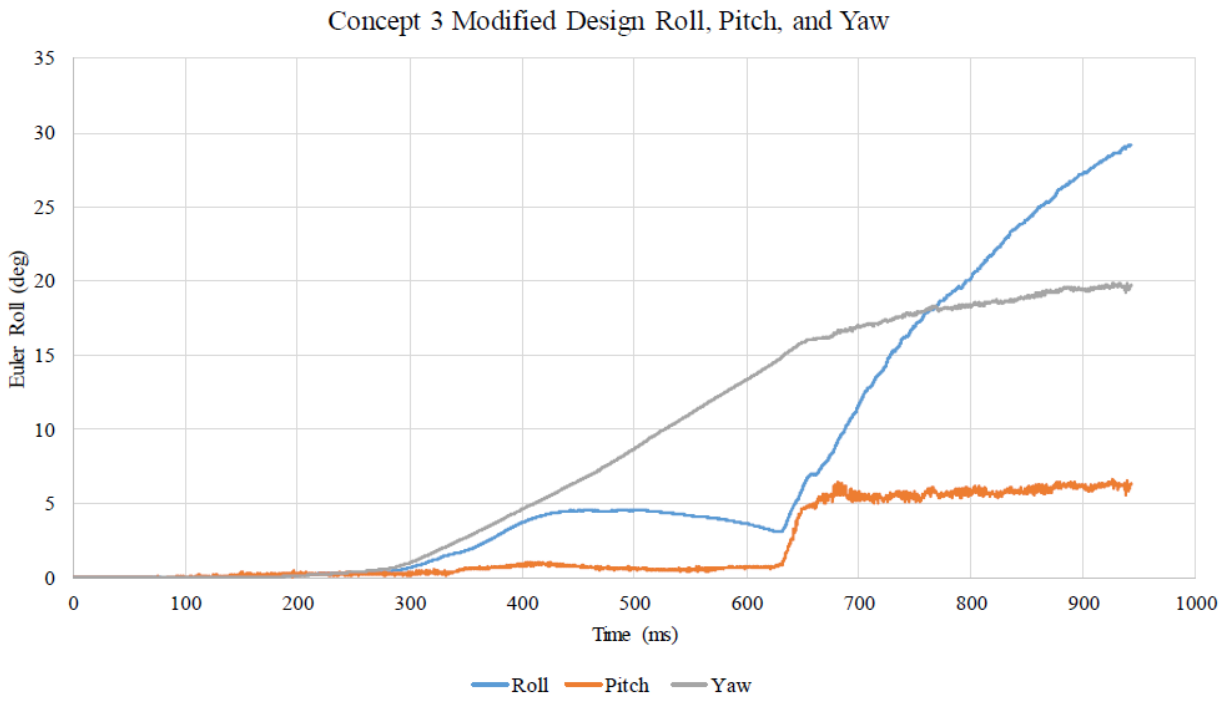

Figure 3.12 TL-6 Angular Displacement of the baseline model [4]

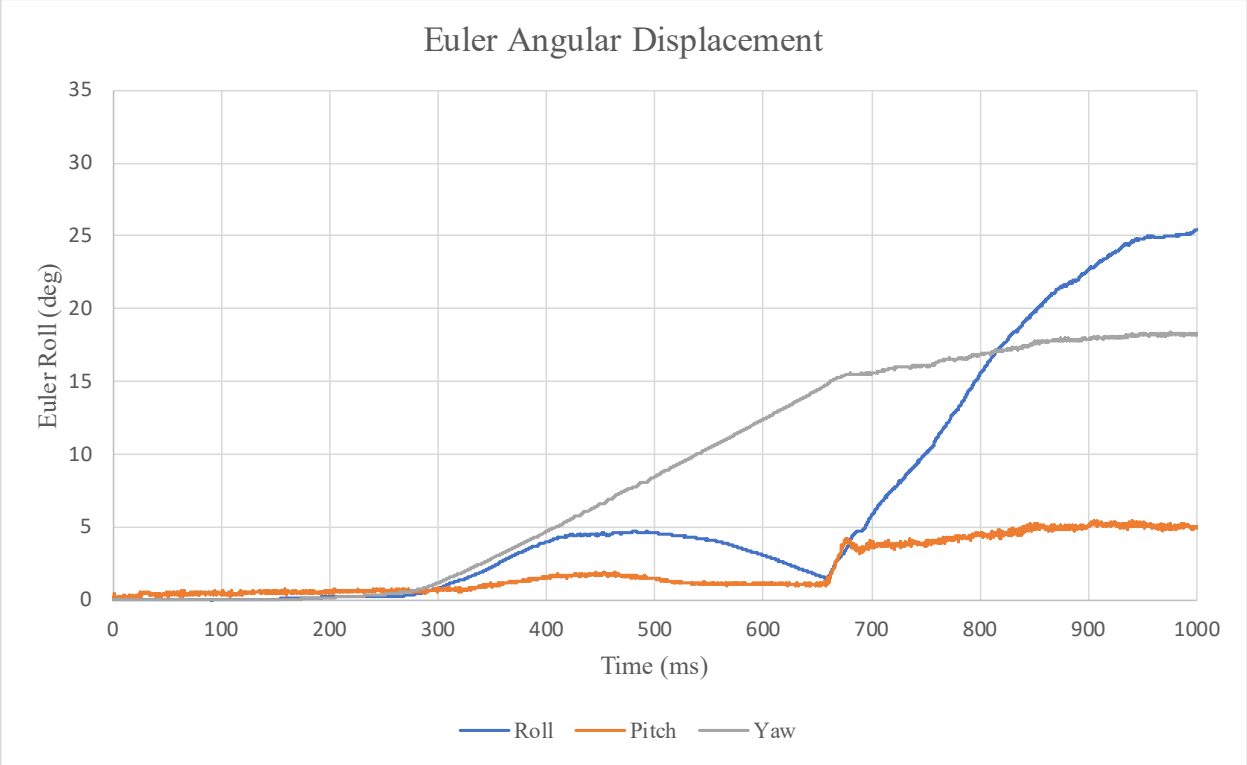

Figure 3.13 TL-6 Angular displacement of the deformable concrete barrier model

Table 3.5 Comparison of angular displacement

Parameter	Rigid Simulation Angle	Deformable Simulation Angle	Deformable Difference Compared to Rigid
Yaw	20 deg	18.4 deg	8% lower
Pitch	6 deg	5.5 deg	8% lower
Roll	29 deg	25.6 deg	12% lower

3.4 Conclusion

The rigid concrete barrier baseline model was modified to have deformable concrete in order to observe any change in performance under MASH TL-6 tank-trailer truck impact condition. The barrier was re-meshed to 1 in. cubic size, rebar was added, and a foundation model was added below the ground level using LS-DYNA. Based on the comparison, the simulation provided reasonable estimates of deformable barriers subjected to the MASH TL-6 impact condition. The barrier model remained intact without noticeable damage on the traffic side or back side. The changes to the model were a 16% reduction in the exerted force and reduced angular roll. Both barriers contained and redirected the truck and showed similar behavior. Either barrier model would be acceptable for a preliminary evaluation of truck containment. The deformable barrier mode is recommended to be used to evaluate concrete damage.

3.5 Recommendation

The Instrumental Wall force result in the TTI report is shown in figure 3.14 [6], and the peak forces from this crash test were compared to the simulation results, as shown in table 3.6. The exerted forces of the Instrumented Wall are significantly higher than the simulation forces with both a rigid concrete and a deformable concrete barrier. The most significant difference was

observed in the 3rd peak force. While it is anticipated that the new TL-6 barrier concept will have forces lower than what was observed in the Instrumented Wall test since it can deform some, the forces still seem unrealistically low. Thus, it is still recommended to develop the trailer model in more detail to determine if more accurate forces can be modelled. The force discrepancy could also be caused by different tractor models. The tractor model used for the Instrumented Wall test was 1973 White Freightliner Tractor, and the tractor model used for the simulation was a much newer model. It is possible that the drastic evolution in the technology of the suspension of the tractors and other technologies within the tractor could make a different result.

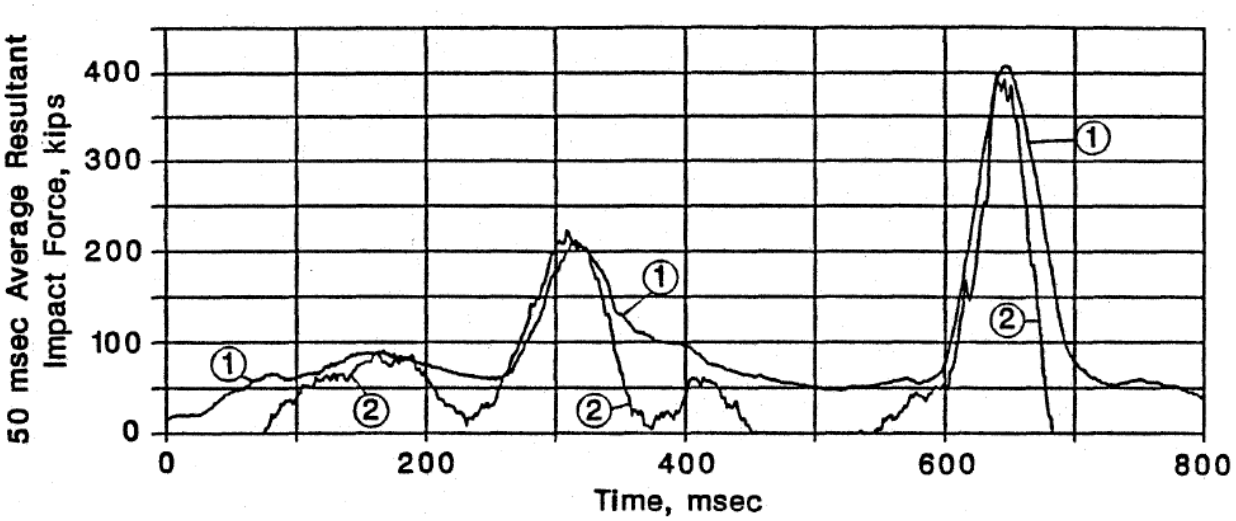

Figure 3.14 Instrumented Wall force [6]

Table 3.6 Peak force comparison

Peak Force Location	Simulation Force	Instrumented Wall Force	Simulation Difference Compared to Test
1st peak	83 kips	91 kip	9% lower
2nd peak	111 kips	212 kip	48% lower
3rd peak	124 kips	408 kip	70% lower

Chapter 4 Finite Element Model Development and Validation

Nonlinear analysis depends on two factors: material properties and geometry. Nonlinear material properties do not follow Hooke's law of the stress-strain curve. Nonlinear materials that have high failure rates, such as water, are modeled in LS-DYNA using *MAT_NULL material with the equation of state (EOS), which imparts additional material properties to simulate more accurately the fluid behavior. Two common types of EOS used for fluid impact analysis are linear polynomial and Grüneisen.

4.1 Vehicle Model Overview

As part of the Year 2 evaluation of the MATC TL-6 barrier, researchers constructed the model of a tank similar to the LBT BKZ 5949 elliptical straight-frame structure, with four independent tanks. The LBT tank structure is shown in figure 4.1. The critical components of the LBT model are shown in figure 4.2.

The TL-6 tank trailer was evaluated to classify each component as critical or non-critical. Critical components were prioritized for accurate geometrical modeling, thicknesses, behaviors, and connections. Trailer components deemed non-critical, which were typically non-structural parts such as hoses and clamps, were excluded from the initial modeling due to complexity and effort to implement each feature. A total of 134 unique, critical components were modeled in the tank trailer model.

A redefined tractor-tank trailer vehicle model was created for LS-DYNA simulation. The following section explains the element details for every component of the tank-trailer model. The tank-trailer compartment has an approximate length of 42-ft 5-in. (12.9 m). The overall tank has capacity of 9,500 gallons, which is divided in four compartments, with each compartment having a capacity of 3,500-1,000-1,500-3,500 gallons from front to rear, respectively.

BKZ 5949

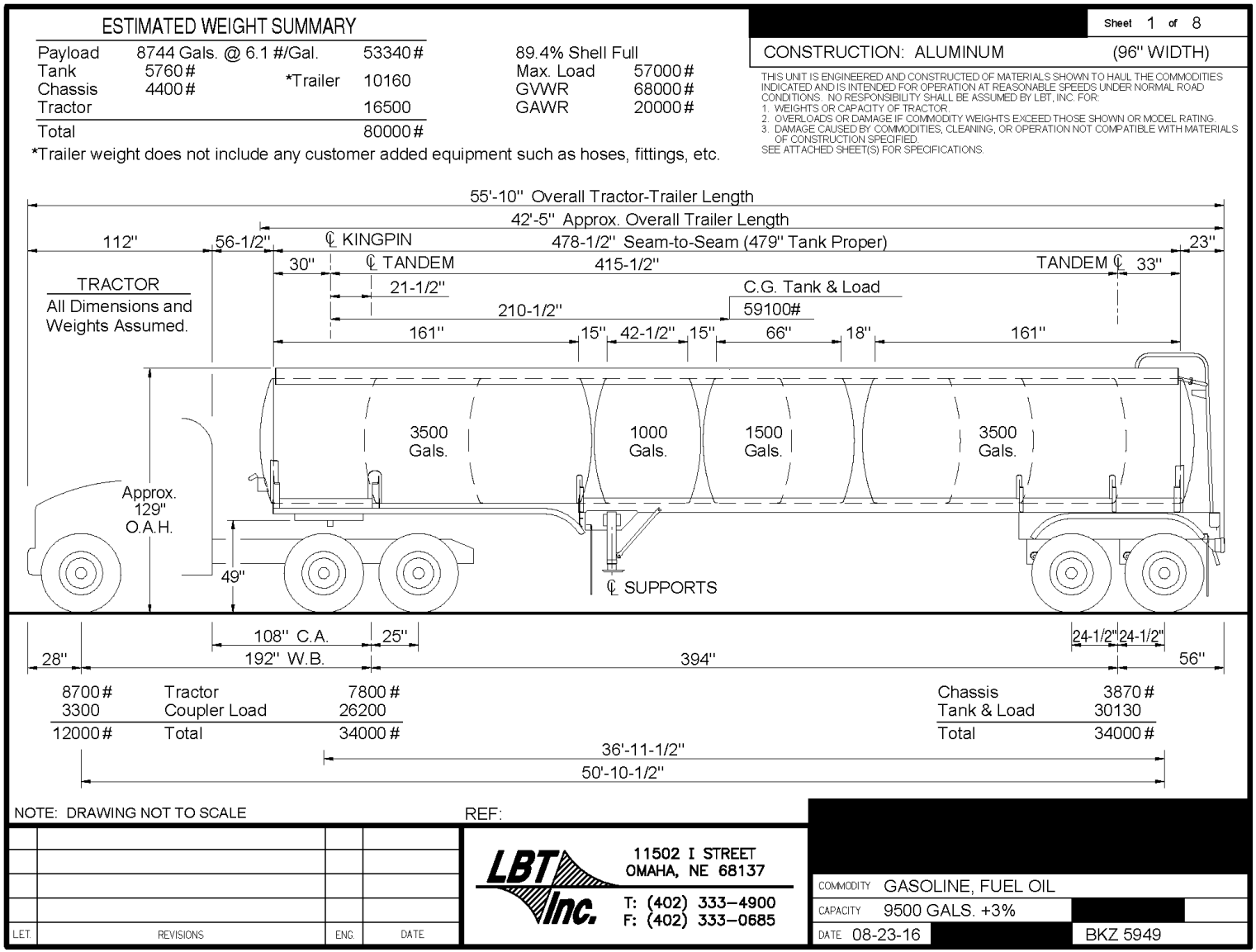

Figure 4.1 Size and Tank Specifications for LBT BKZ 5949 Elliptical Straight-Frame Tank Structure

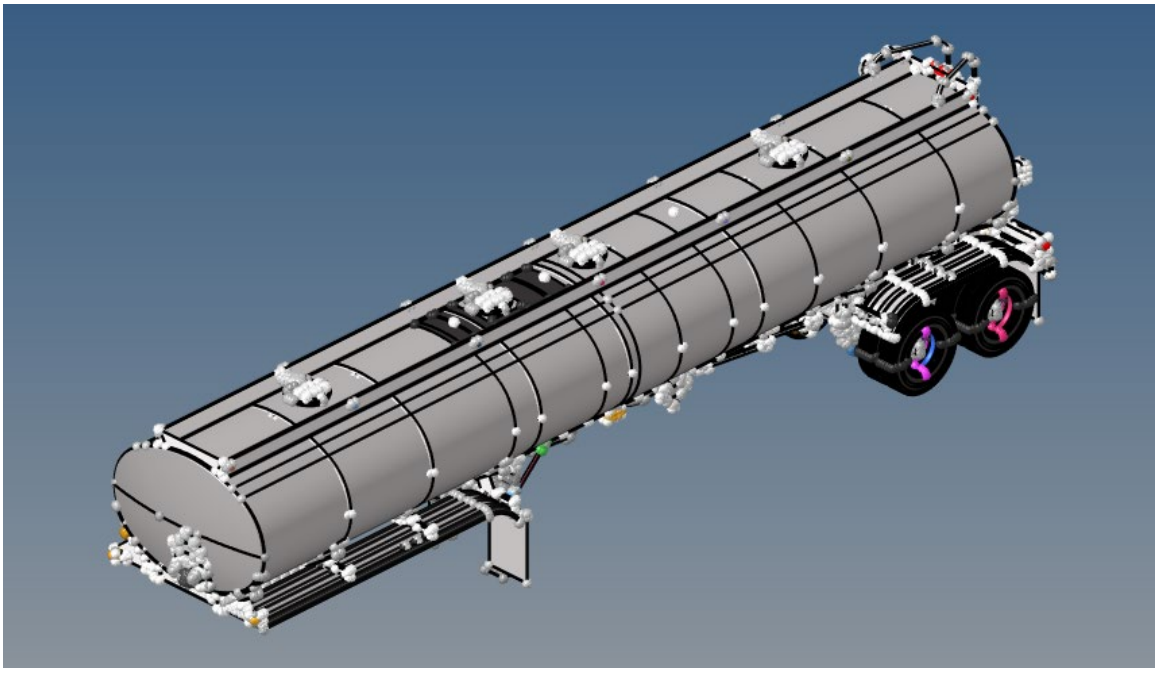

Figure 4.2 TL-6 Tank 3D Model

4.1.1 Critical Components Included in Model

The critical components were defined as the parts from the tank-trailer that are structurally essential for the analysis when simulating the tractor-tank trailer impaction into the TL-6 barrier. These components are the baffles, bulkheads, shell, and chassis frame that are shown in figure 4.3.

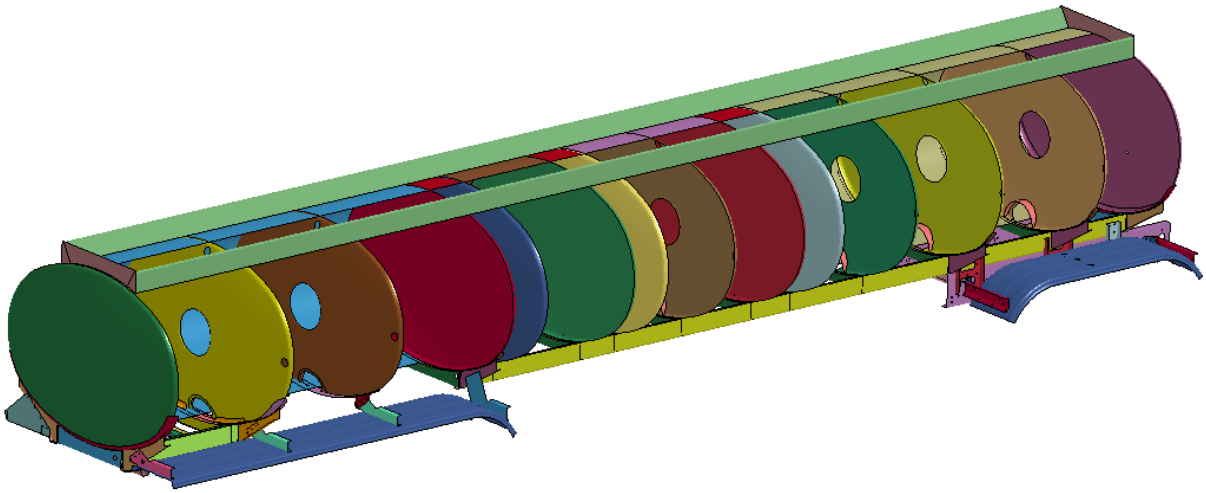

Figure 4.3 Critical Components (External Tank Not Shown for Clarity)

4.1.2 Excluded Components

As discussed, non-critical components were those which were not believed to have a significant effect on the dynamics, weight, or behavior of the tank trailer. These components include the hoses, wires, gaskets, light structures, wires, and some tubing structures. Future applications of this model could include these components deemed non-critical if need arises.

The highly detailed components are the parts of the model that have a complex geometry, some of these components were the spigots and valves, molded components, bolts, and taillight structures, which are shown in figures 4.4 and 4.5.

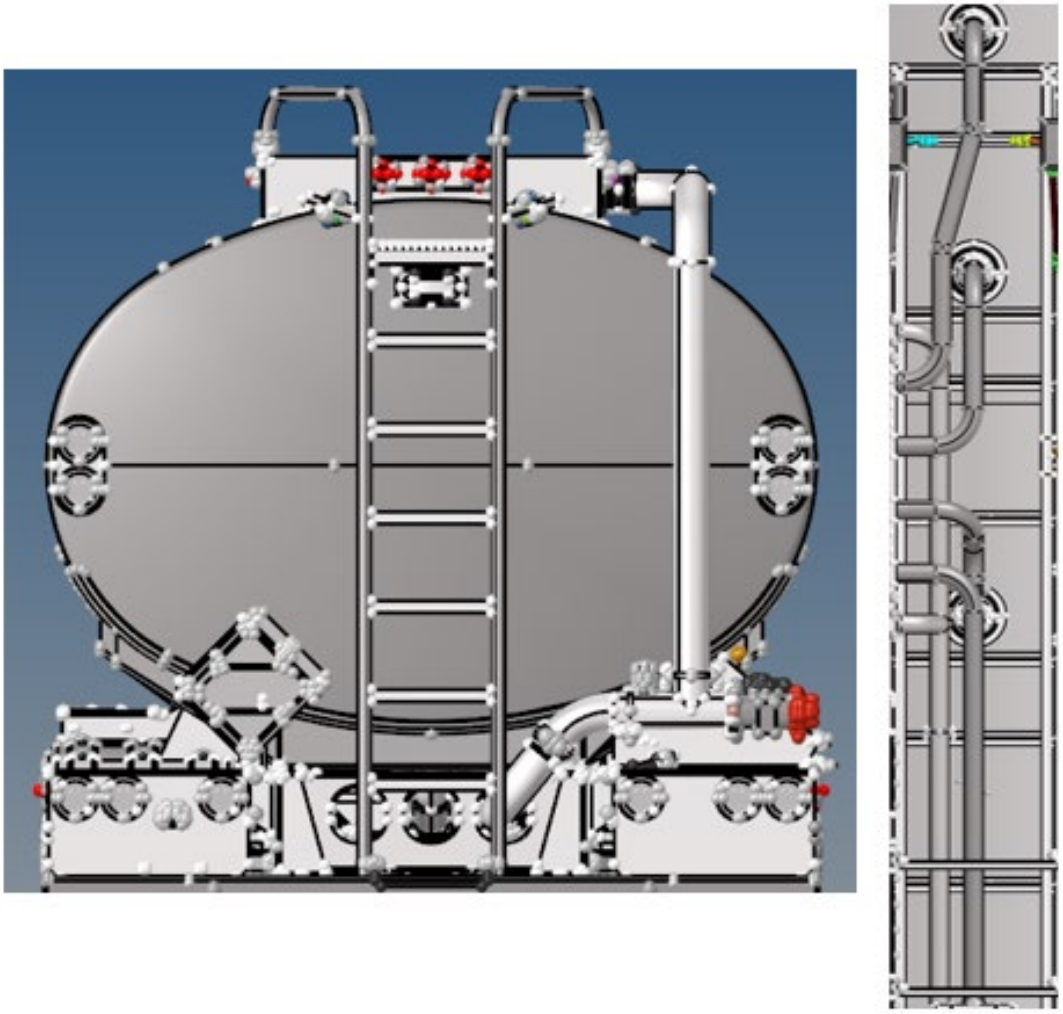

Figure 4.4 Examples of Non-Critical Components

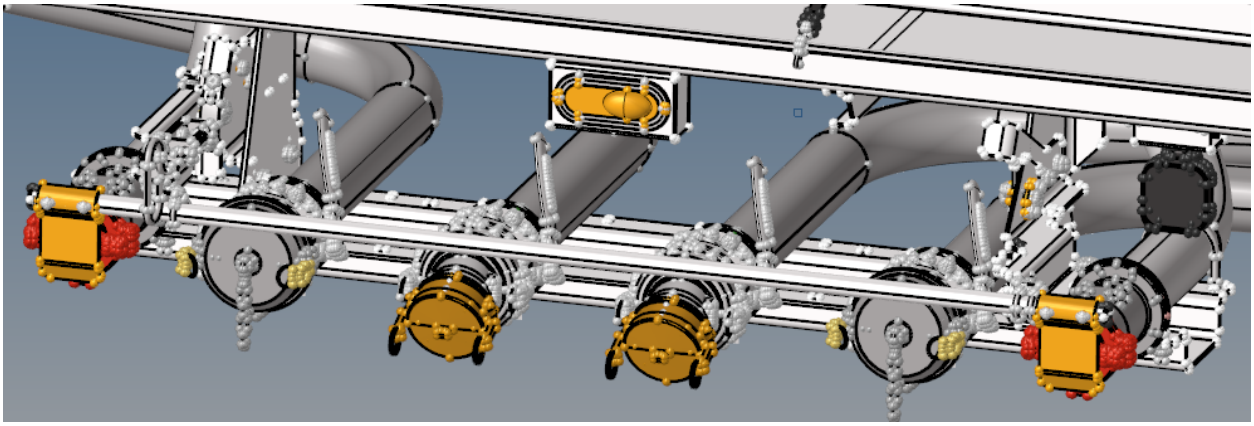

Figure 4.5 Examples of Non-Critical Components

4.2 Components Overview

After categorizing the components from the tank-trailer model, the following step was to generate the mesh for each part in the model. This consists of subdividing the geometry in small elements. The tank model consisted of two different types of elements: shell and solid. Shell elements were used to model most of the parts throughout the tank trailer. Other components from the vehicle model were solid elements, such as the pin located in the fifth wheel, which connects the tank trailer to the tractor.

4.2.1 Baffles, Bulkheads and Shell

The fluid tank structure consisted of an exterior elliptical aluminum skin (tank) which were welded to tank end caps (bulkheads) and slosh-resistant interior rib stiffeners (baffles). These components from the tank trailer are fully integrated Belytschko-Tsay (B-T) shell elements, which is computationally efficient due to the reduced number of integration points used. These tank components were the most critical components and are the only components which directly interact with the modeled tank fluid. The modeled tank structure is shown in figure 4.6.

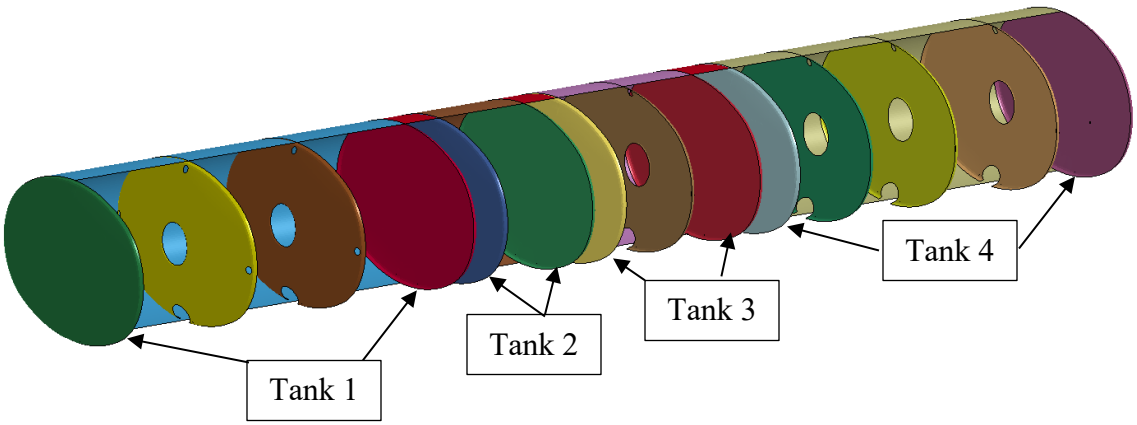

Figure 4.6 Tank Shell (partially hidden for clarity), Bulkhead, and Baffle Structures

The tank was modeled in five parts, one for each closed-volume tank and one for the connecting skin between tanks. The tank structure is shown in figure 4.7.

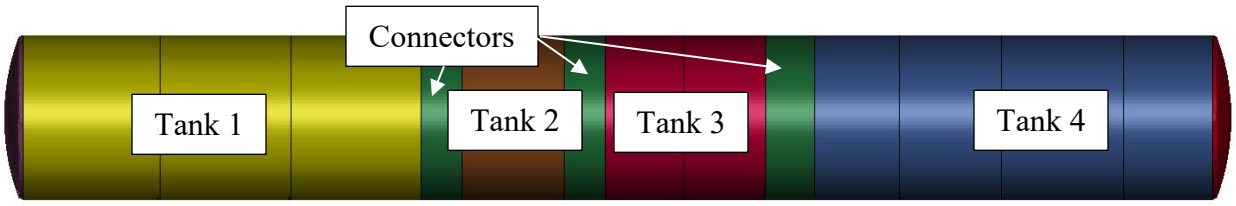

Figure 4.7 Tank Components

The bulkheads and baffles were meshed with similar shell element structures. To accomplish this, researchers meshed baffles and added void surfaces between openings in the components. The mesh was then extended to the bulkheads. As a result, the meshes for all baffle and bulkhead structures were consistent throughout the tanks from front to rear. The average element edge size of the baffle and bulkhead structures was approximately 25 mm. The bulkhead and baffle meshes are shown in figure 4.8.

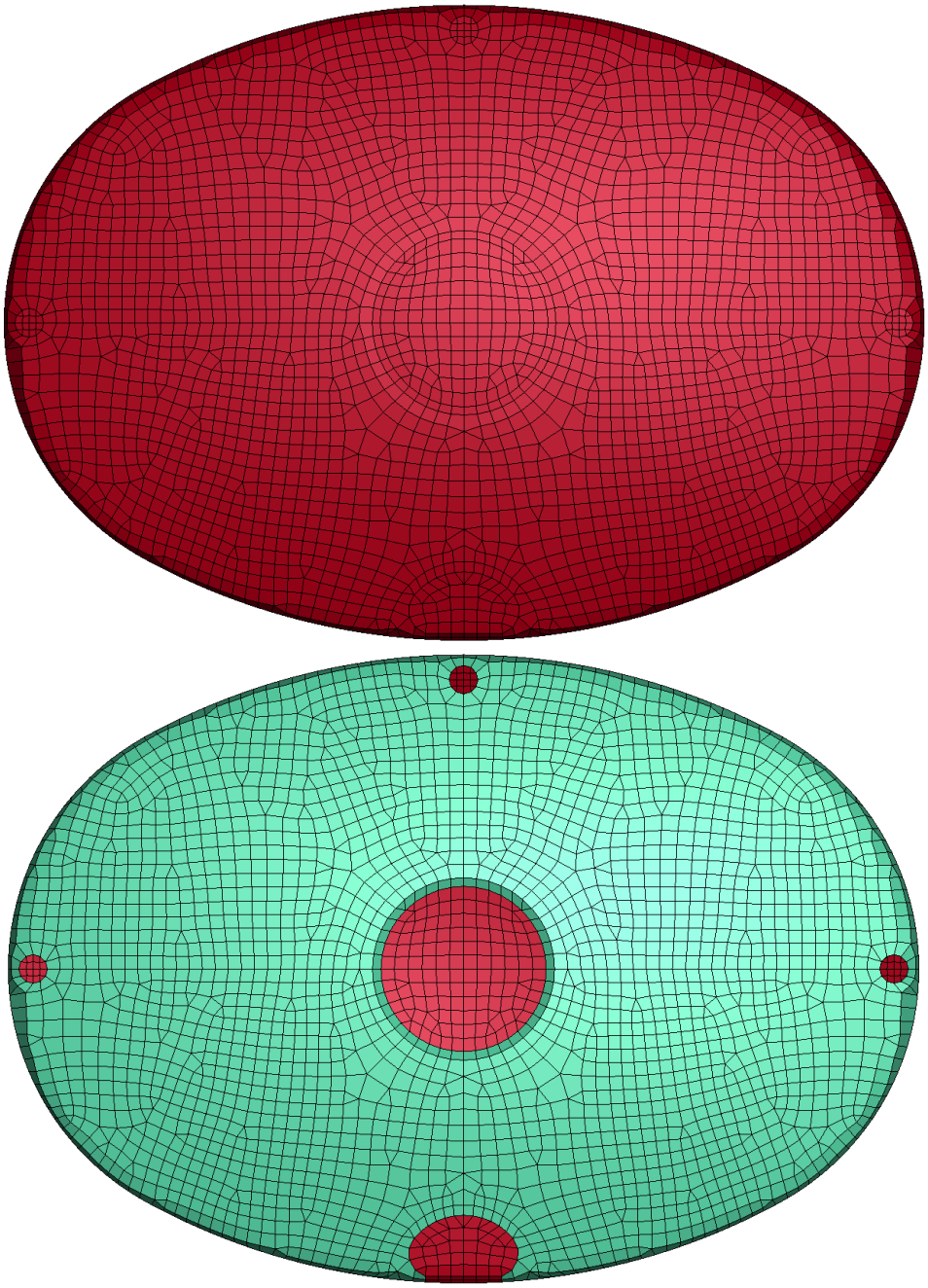

Figure 4.8 Bulkhead (top) and Baffle (bottom) Meshes

4.2.2 Chassis Frame

The tank, bulkhead, and baffle structures were mounted to a chassis frame components were modeled with B-T shell elements. Two main chassis sections were welded to the underside of the tank structure as stiffeners to assist with supporting the fluid weight. The fluid structures

consisted of flat flanges welded to rib structures and spanning between two longitudinal rails. Two thin shells were also attached to the chassis on the left and right sides corresponding to the tops of the wheel structures.

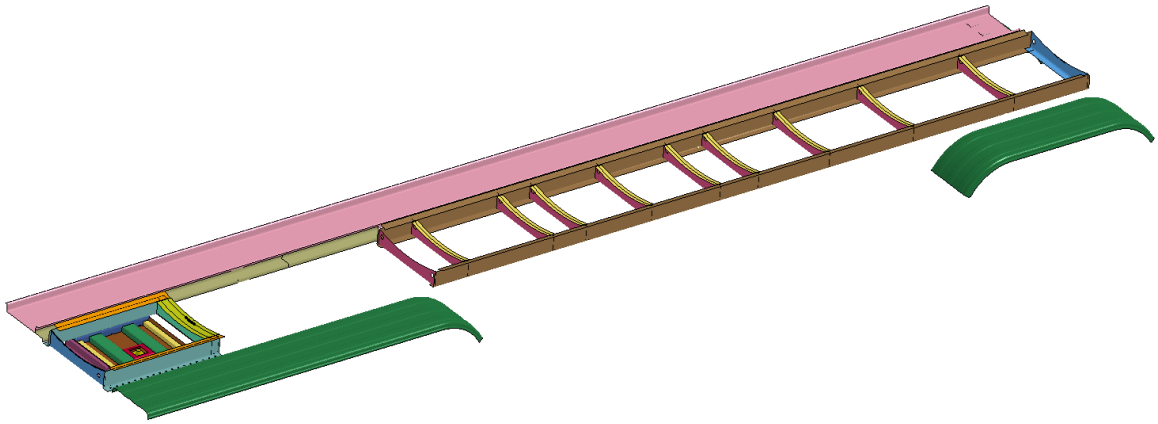

Figure 4.9 Chassis Frame

4.2.3 Fifth Wheel

At the front of the trailer, a fifth-wheel load frame and shear pin were modeled based on the details provided by LBT Inc. A fifth wheel pin structure is a common method of attaching heavy trailer structures to tractors, and a similar structure is used in tractor and box trailer combination vehicles. The fifth wheel shear pin was modeled with solid elements and secured to the rib, frame, and strut members of the fifth wheel box. The fifth wheel system is of great importance since it connects the tank to the tractor. This component is modeled with solid elements. The fifth wheel shear pin and load frame models are shown in figure 4.10.

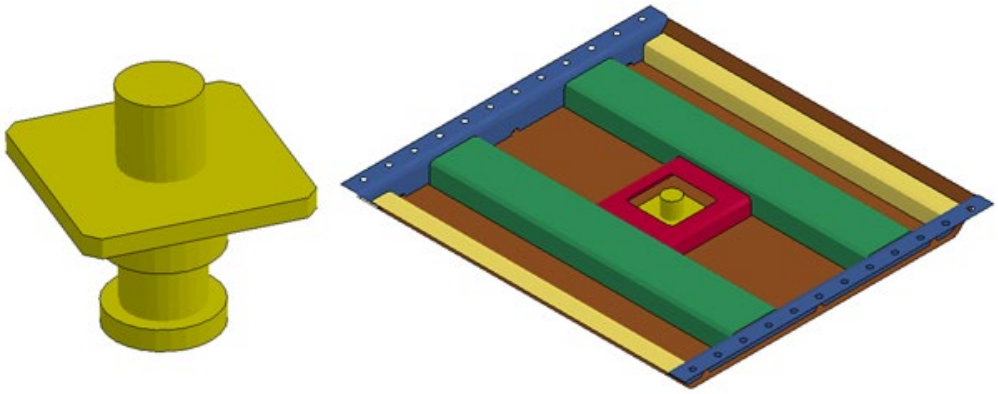

Figure 4.10 Fifth Wheel Shear Pin and Load Frame

4.2.4 Suspension and Wheel System

The suspension is among the most complicated structures in most vehicle and trailer models. Part geometries, connections, joints, and interactions require careful detail and consideration.

The suspension of the trailer system was compared to existing vehicle and trailer models. It was observed that the TL-6 model had very similar structure, including air ride suspension, trailing arm assembly, dual axle support, and height as the existing TL-5 box trailer system. Therefore, researchers modified the geometry of the TL-5 rear suspension to match the height, connections, depths, and reinforcement of the TL-6 trailer and mounted the connection points at similar locations to the chassis. The modified TL-5 suspension system which was used in the TL-6 tank trailer model is shown in figure 4.11.

Most of the components from the suspension and wheel system are fully integrated shell elements. The components that are considered to be a constant-stress solid elements are the suspension pivot, air bag supports and accelerometer. The rear shock absorber, air ride spring and air ride damper were modeled with discrete elements.

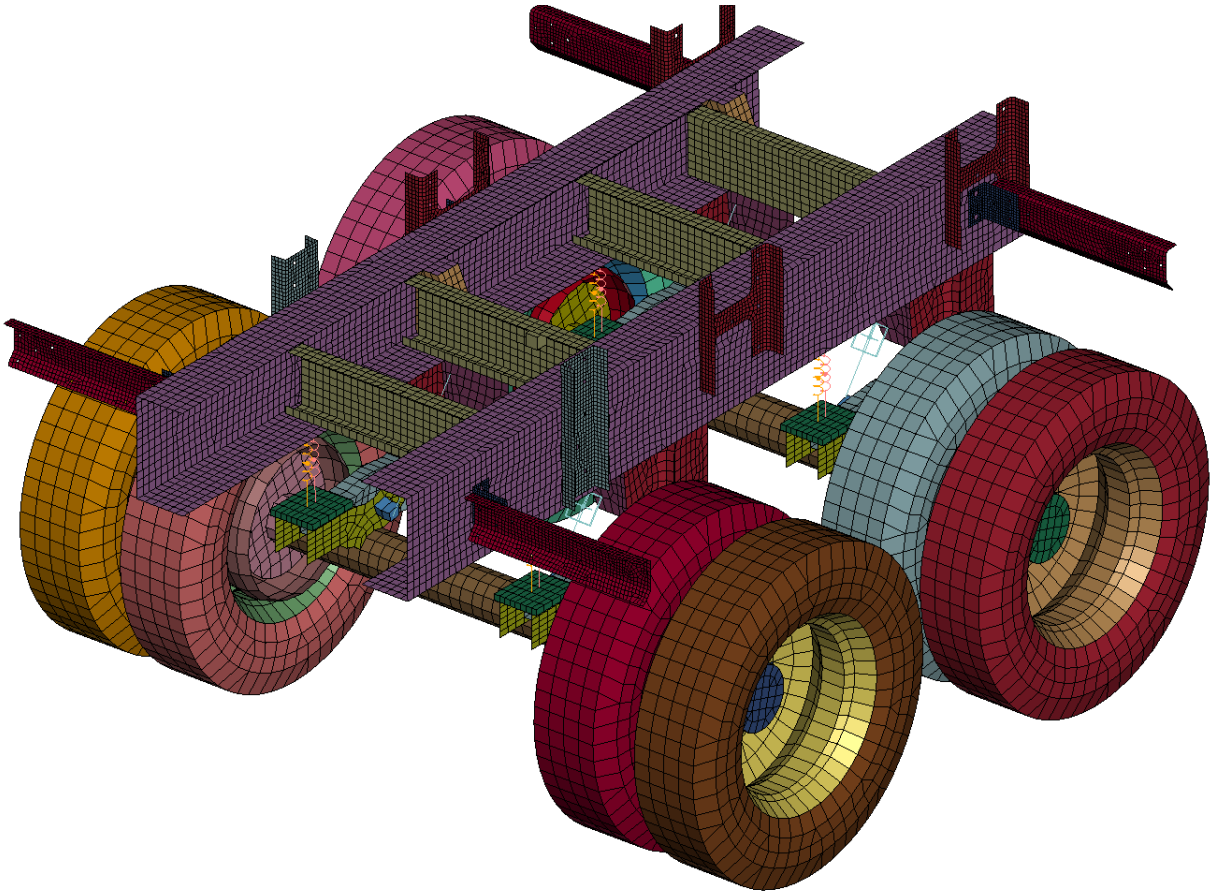

Figure 4.11 TL-6 Rear Suspension Model Modified from TL-5 Box Trailer

Chapter 5 Material Modeling

5.1 Material Overview

The mechanical properties of different types of aluminum alloys were applied to the tank-trailer model. Material selection was based on guidance for structural container specifications for road vehicles, as noted in Aluminum in Commercial Vehicles [14]. The reason why different types of materials are used to model the tank is that each of the components has a different function in the model, which can go from giving structural support to containing hazard materials that could be corrosive or explosive. The materials and properties used in the material sections are shown in table 5.1.

Table 5.1 Aluminum Mechanical Properties

Material	Density (kg/mm^3)	Young's Modulus (Gpa)	Poisson Ratio	Yield Strength (Mpa)
5454-O Al	$2.69(10^{-6})$	69	0.33	100
5454-H32 Al	$2.69(10^{-6})$	69	0.33	200
6005A T5 Al	$2.70(10^{-6})$	69	0.33	250
6060 T6 Al	$2.71(10^{-6})$	68	0.33	170
42000 T6 Al	$2.60(10^{-6})$	70	0.33	220

No tensile sample or stress-strain curves were available for any material models used in this tank. Initial material models used a bilinear plasticity definition. It is expected that material refinements to this tank model will include accurate true stress-true strain definitions for all materials.

5.2 Baffles and Bulkheads

The type of aluminum alloy for the baffles and bulkheads is 5454-O Al, which was provided by a tank description document from LBT Inc., this type of aluminum is commonly used in welded structures such as pressure vessels and has a very good corrosion resistance.

Material properties were approximated based on ASTM specifications and estimated yield and ultimate stresses.

5.3 Outer Shell

5454-H32 Al alloy was selected to represent the material properties of the outer shell in the model. This material has a very good corrosion resistance, and heat treatment and fabrication techniques can alter strength from medium to high with a high fatigue strength. The alloy has a good strength at high temperatures (65-170 degrees Celsius). The characteristics are proper for the component function, which is to contain the fluid and do not let it spill out of the tank.

5.4 Chassis Beam

For these components the material properties from 6060-T6 Al alloy were used in the vehicle model. This type of aluminum is commonly used for complex cross-section and has a very good weldability. These characteristics are a right fit for the chassis beam due to a complex cross-section and function of the component, which is to give structural support to the tank.

5.5 Chassis Components

The 42000 T6 Al material properties were designated to the components in the model that are used to as an intermediate to connect different parts to each other. Most of these components are bolted to other components.

Aluminum 6005A T5 material properties are designated to the L-beam components in the model. This medium strength aluminum alloy is corrosion resistant and is used for structural applications, typically used in truck, trailer and automotive vehicles.

Chapter 6 Connections, Constraints, and Contacts

6.1 Connections

Researchers extensively referenced the LBT Inc. tank model to identify the best techniques for connecting critical components in the tank model. Different connection types were utilized based on how parts were connected in physical trailers. Welded connections were modeled by either merging nodes of welded parts or defining spot welds. When meshes of adjacent components were non-conducive for spotwelds, researchers applied tied node interfaces to link components. Bolted connections were independently analyzed. When bolt arrangements restricted part rotations and could develop moment in connections, researchers applied nodal rigid bodies to interface components. For bolted connections in which rotation or angular displacements could occur, joints or nodal constraints were used to allow relative movement between the connected parts. Connection diagrams shown in figures 6.1 through 6.3 demonstrate the connections for each component in the actual tank-trailer and the LS-DYNA model.

LBT manufactures tanks with the baffles and bulkheads welded to the outer shell and evaluated to ensure no fluid passes through the weld or around critical tank structures. Contact between these components is of major importance because these parts contain the fluid. The edges of the bulkheads and baffles were modified and matched the mesh of the tank so that the meshes could use merged nodes. When nodes could not be merged, tied nodes were used to link shell edges together.

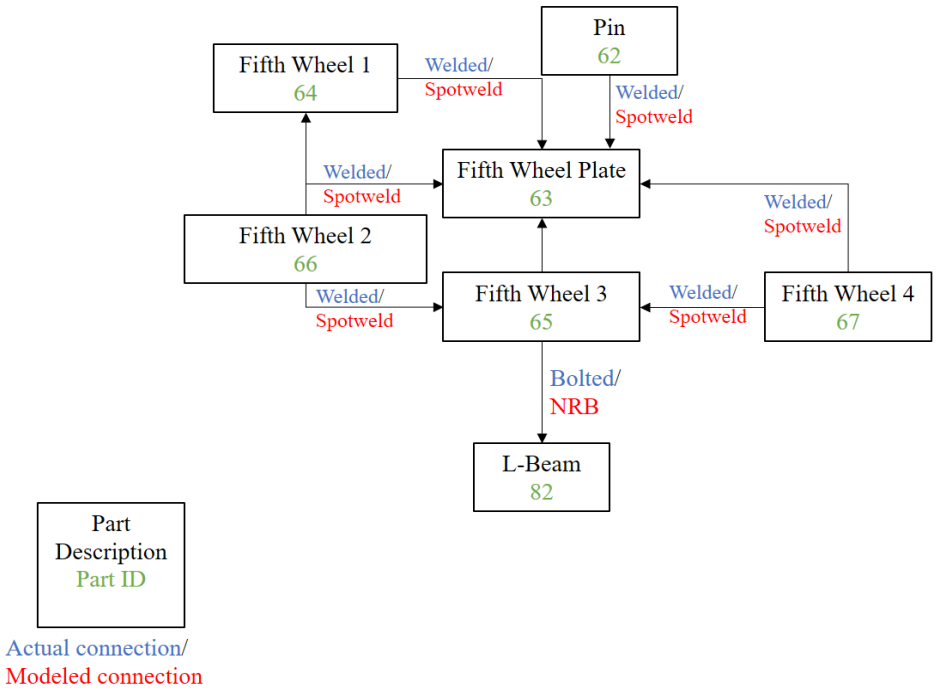

Figure 6.1 Fifth Wheel Connection Diagram

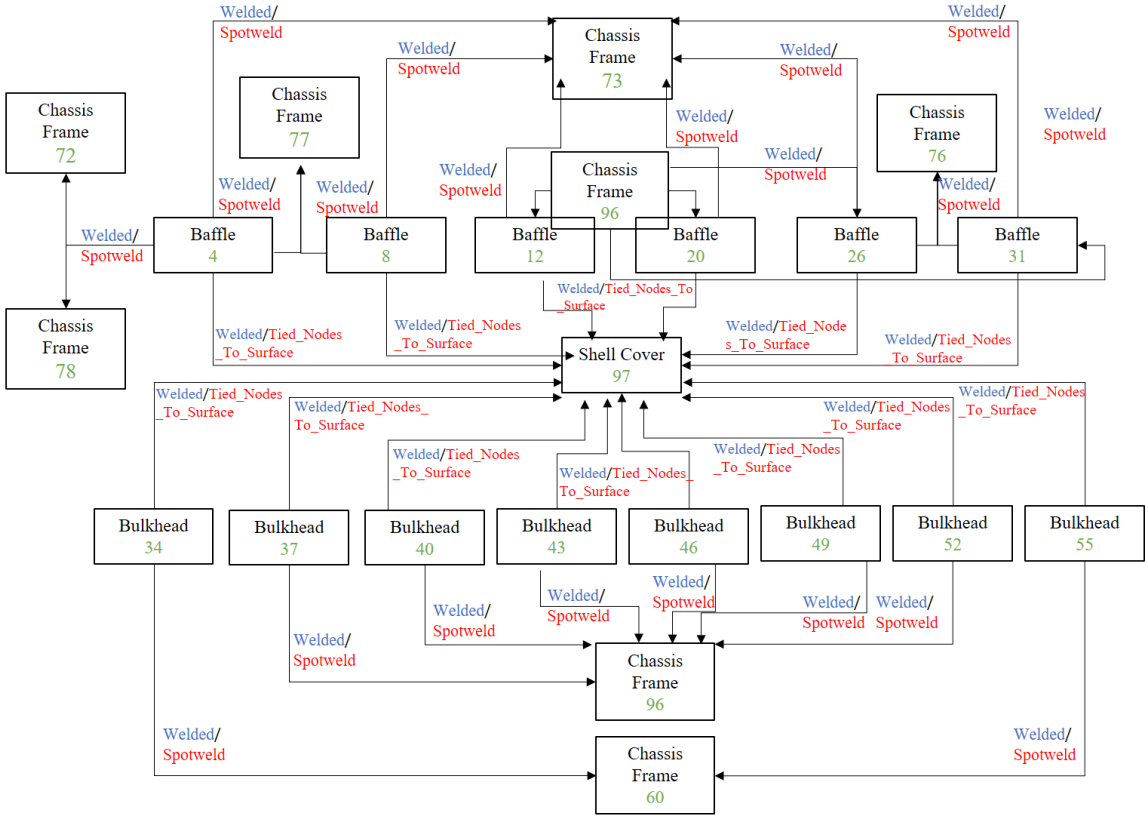

Figure 6.2 Tank Connection Diagram

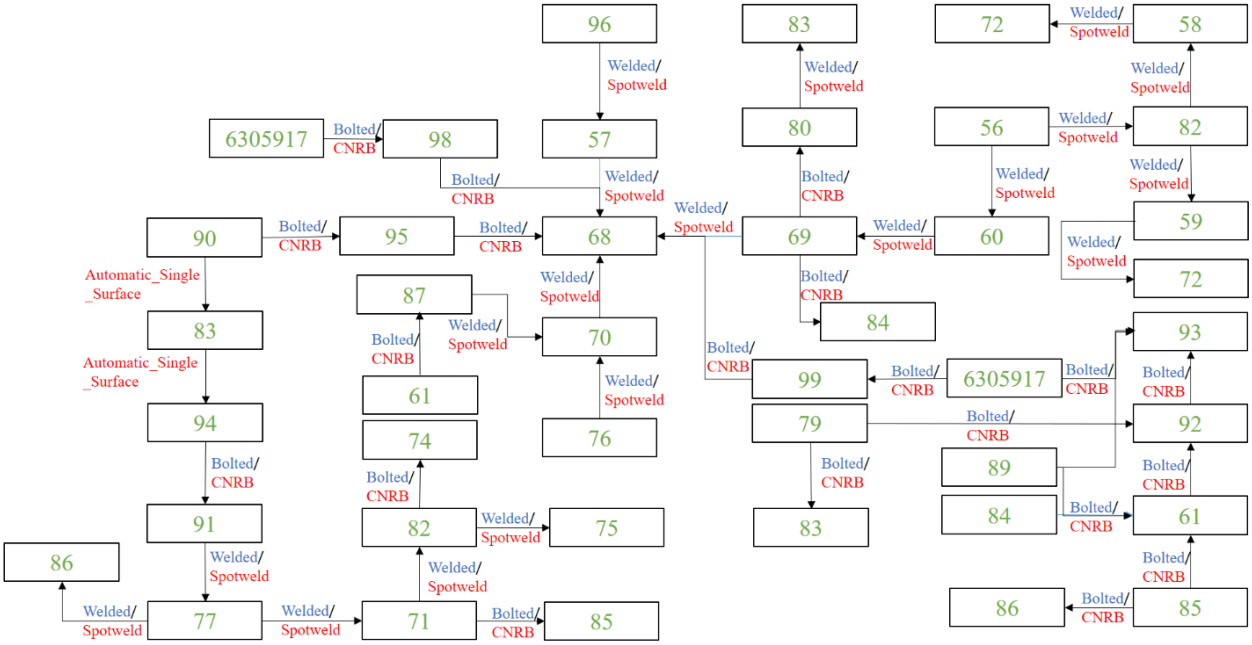

Figure 6.3 Chassis Frame Diagram

6.2 Contacts

*CONTACT_AUTOMATIC_SINGLE_SURFACE was used for most structural components in the model. This type of contact is widely used for crashworthiness applications. For this type of contact the slave surface is typically defined and no master surface is defined. The contact is considered in all parts in the slave section.

A separate contact group was applied for baffles and interior bulkheads, tank, and fluid models. The interior tank components did not interact with the exterior contacts outside of the trailer and thus were not included in the overall tank structure.

6.3 Joints and Constraints

Few explicit joints were modeled in the tank model. Most joints were located in the suspension structure. Each wheel joint was modeled with a pair of spherical joints, using nodes attached at the axle locations. The trailing arms of both front and rear axles were pinned to the

chassis using a similar pair of spherical joints. This technique was extensively used in the TL-5 trailer suspension, as noted.

The spring and shock elements of the suspension connected critical nodes on the axle frames and the chassis components. The connections and force-displacement properties of each component were closely matched to corresponding elements in the TL-5 trailer model.

Chapter 7 Fluid Modeling

7.1 Introduction

The literature review identified many potential fluid modeling techniques. Four fluid models were explored and are described in the following sections. The four fluid models described below are Lagrangian Simple Fluid; ALE; SPH; and DES. Further research is recommended to determine which model performs the best.

7.2 Lagrangian Simple Fluid

The Lagrangian Simple Fluid model consisted of solid element mesh mapped within the tank structure. The solid element mesh was constructed by dragging the shell interface of the bulkhead to the interface of the baffle and discretizing with an average element length of 40 mm. The solid element mesh is shown in figure 7.1. The fluid material was modeled using MAT_002, or MAT_ELASTIC_FLUID.

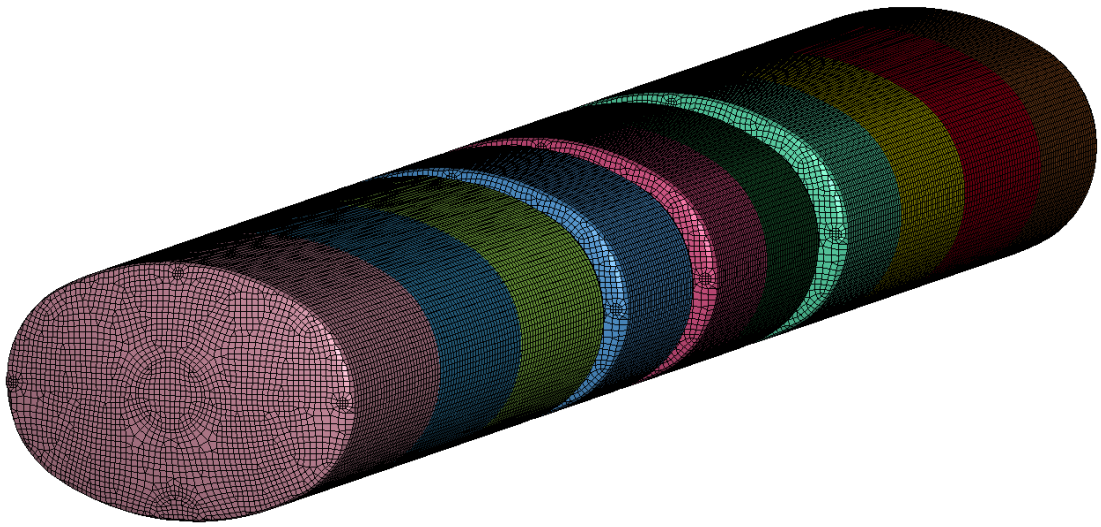

Figure 7.1 Simple Solid Element Fluid Model

7.3 ALE Modeling

After researching and comparing the different types of computational methods to create and analyze the sloshing behavior of a fluid, the ALE method was believed to provide an accuracy improvement over the simple solid element fluid model. This method is relatively computationally inexpensive and there is less mesh distortion, which could reduce potential model instabilities. A redefined fluid model was created for LS-DYNA simulation. The following section explains the element details for every component of the fluid model. The model of the fluid is shown in figure 7.2. The fluid is divided in four sections, which is the number of compartments in the tank-trailer. The model has two types of fluids: Water and Air.

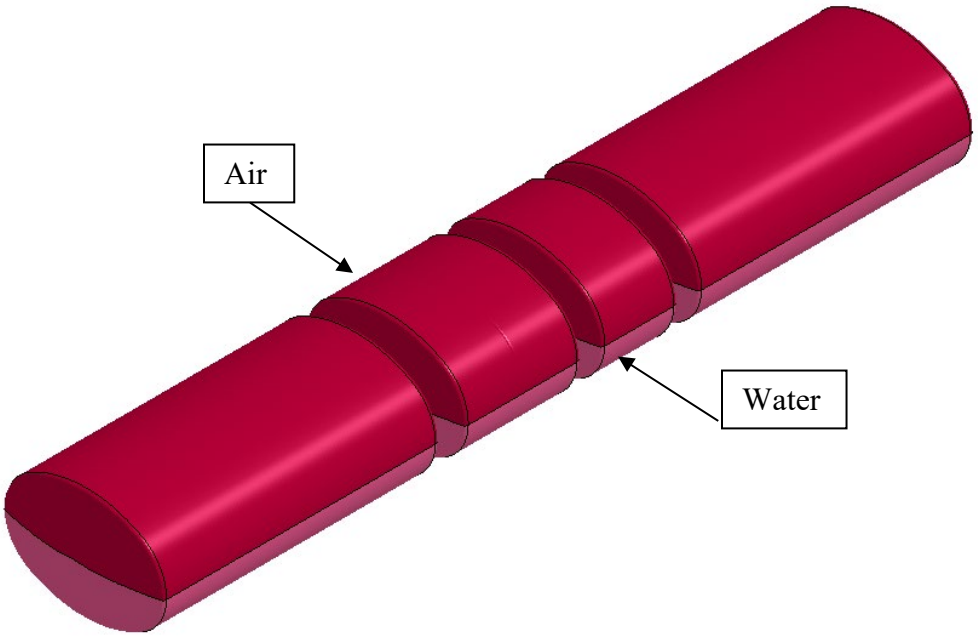

Figure 7.2 ALE Fluid Model

7.3.1 Water and Air Model

Due that the physical process of the model involves fluid behavior, the model for the fluid consist of solid elements and the element formulation is specified to be one point ALE

multi-material for both water and air. The material properties assigned to the liquid model were for water at room temperature (72°F), a density of 1.0E-6 kg/mm^3. For the air, the material properties assigned were a density of 1.225E-9kg/mm^3. Other material properties are defined in table 7.1.

Table 7.1 ALE Multimaterial Fluids Material Properties

Property	Water	Air
EOS	Grüneisen	Linear Polynomial
Density (kg/mm^3)	1E-6	1.225E-9
Pressure Cut-off (Kg/m.ms^2)	-100	-
Viscosity Coefficient	8.68E-4	1.252
Bulk Modulus (GPa)	2.25E-8	-
Initial Internal Energy (E_0)	0	0
Initial Relative Volume(V_0)	1	1

7.3.2 Equation of state (EOS)

The equation of estate are used to accurately simulate the material behavior when in simulation. For the water model the equation of state used is the Grüneisen, which is used to simulate liquid behavior. The Grüneisen equations of state defines the pressure of compressed materials as [10]

$$p = \frac{\rho_0 C^2 \mu[1 + \left(1 - \frac{\gamma_0}{2}\right)\mu - \frac{a}{2}\mu^2]}{[1 - (S_1 - 1)\mu - S_2\frac{\mu^2}{\mu + 1} - S_3\frac{\mu^3}{(\mu + 1)}]^2} + (\gamma_0 + a\mu)E \qquad (7.1)$$

Table 7.2 Equation of motion Grüneisen

Velocity of Sound, C (mm/ms)	1500
Grüneisen Gamma (γ_0)	1.65
Volume Correction (a)	0
Coefficient (S_1)	1.79
Coefficient (S_2)	0
Coefficient (S_3)	0

For the air model the equation of state used in the model is *EOS_LINEAR_POLYNOMIAL, this type of equation is used to simulate the behavior of a gaseous fluid [10]. The pressure is given by:

$$P = C_0 + C_1\mu + C_2\mu^2 + C_3\mu^3 + (C_4 + C_5\mu + C_6\mu^2)E \tag{7.2}$$

The linear polynomial equation of state when used to model gas applies the gamma law equation of state [10]. This is achieved by setting the equation as the following

$$C_0 = C_1 = C_2 = C_3 = C_6 = 0 \tag{7.3}$$

And

$$C_4 = C_5 = \gamma - 1 \tag{7.4}$$

Table 7.3 Equation of motion Linear Polynomial

Coefficient C_4	0.4
Coefficient C_5	0.4
Gamma, γ	1.4

7.4 SPH Model

Tank volumes were extracted between different compartments of each tank. Each volume was independently mapped using SPH elements with an average nodal spacing of 50 mm. The SPH models allow a variable fill factor within the tank and apply node-to-surface contact types for all SPH elements. The SPH fluid mesh is shown in figure 7.3.

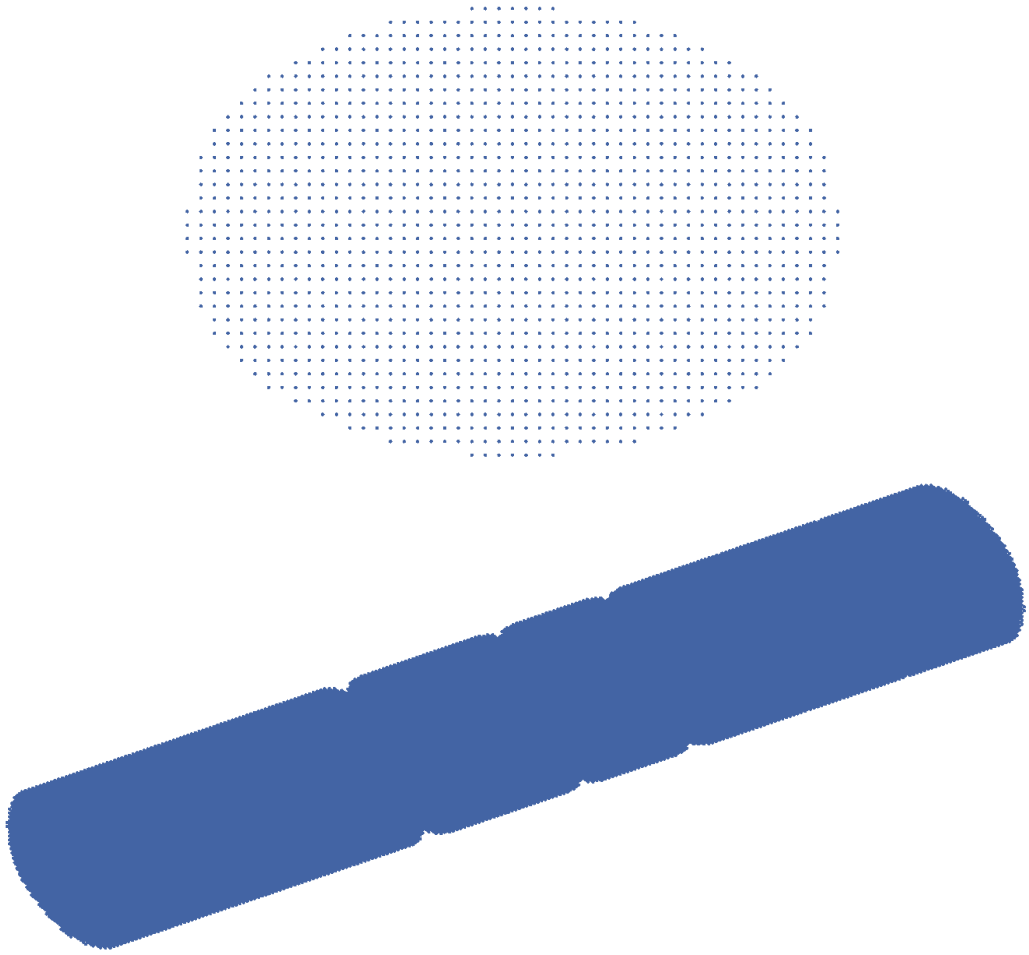

Figure 7.3 SPH Fluid Model Node Distribution

Using SPH models require the use of additional control keywords. Researchers applied bulk viscosity controls and used an Munaghan equation of state:

$$p = \kappa_0 \left[\left(\frac{\rho}{\rho_0} \right)^{\gamma} - 1 \right] \tag{7.5}$$

Where:

p = pressure, GPa

κ_0 = coefficient = $1.5(10^{-4})$

ρ = density (instantaneous)

ρ_0 = initial density = $1.0(10^{-6})$, defined in the material section

γ = scalable modifier = 7.0

The material used with the SPH model was *MAT_NULL which only denoted a nominal viscosity coefficient of $1(10^{-9})$ and a density of $1.0(10^{-6})$ kg/mm^3.

7.5 DES Model

The final fluid model utilized discrete element spheres. As with the SPH model, the tank was partitioned into discrete sections between baffles, bulkheads, and tanks. The LS PrePost DES solver was used to apportion the volume into a compacted matrix of different sphere sizes ranging from 40 to 60 mm in diameter. An image showing the compacted mesh within one tank segment is shown in figure 7.4. The full DES model fill is shown in figure 7.5.

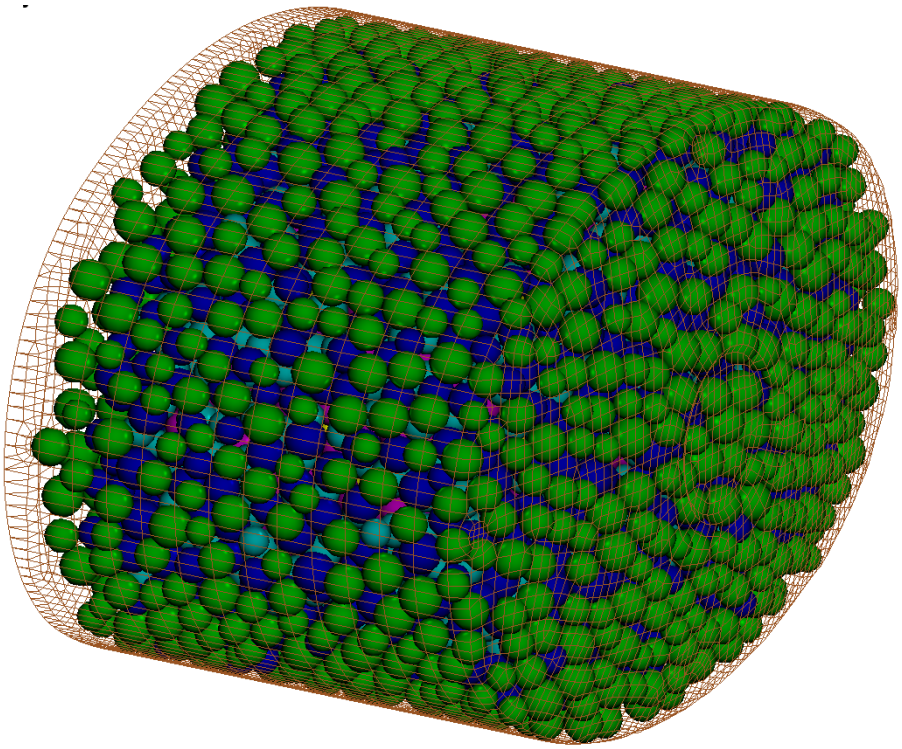

Figure 7.4 DES Model Sample Sphere Fill

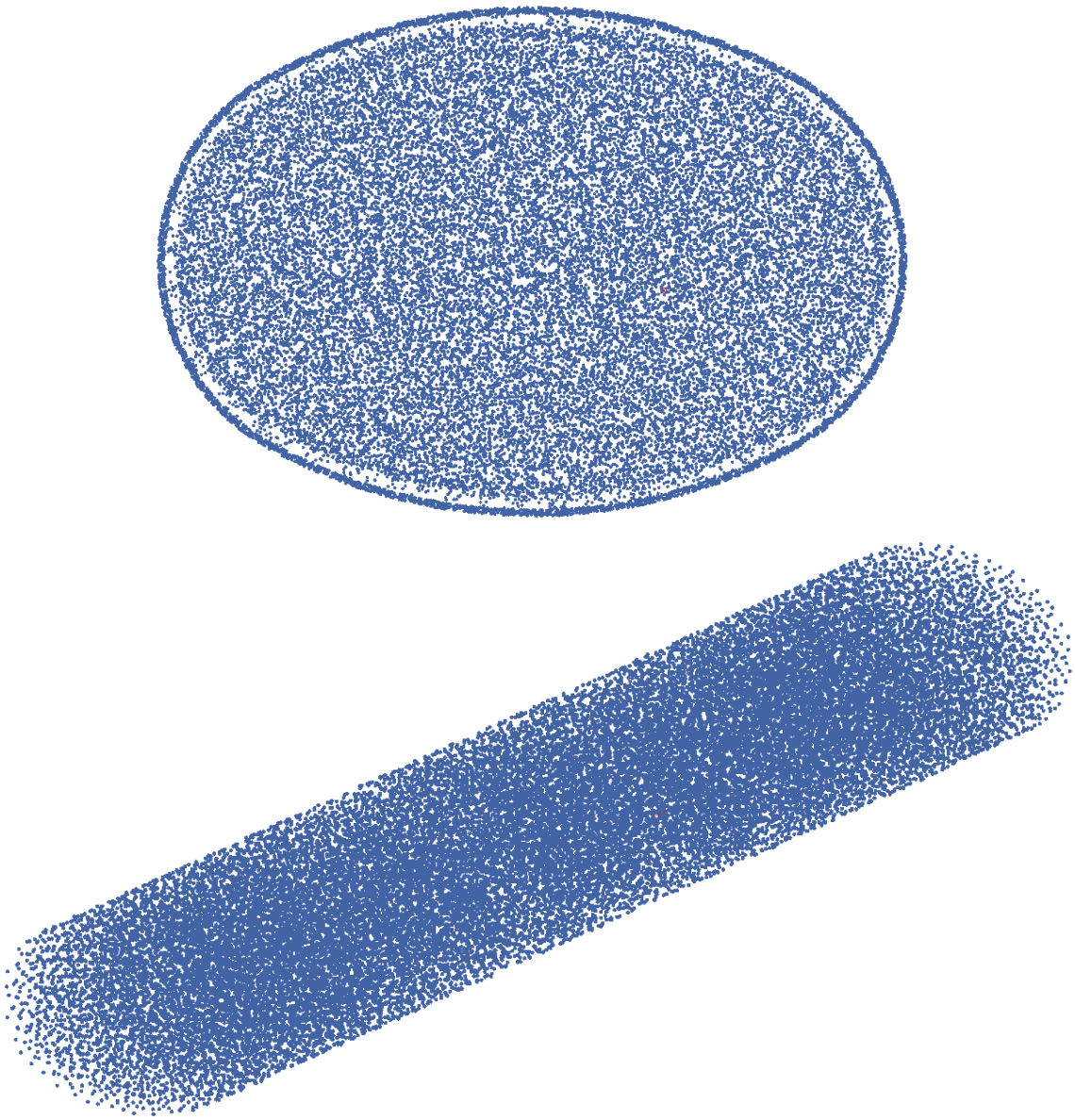

Figure 7.5 DES Nodal Fill

The properties of each sphere, including mass, volume, and size, are appropriated automatically using the DES solver. However, material properties are yet to be determined. Researchers will apply several material models and parameters to the DES model during the Year 3 evaluation of optimized fluid structures and evaluation of tank loading.

Chapter 8 Summary, Conclusion and Recommendations

The objective of this research project was to develop an accurate tank-trailer model for LS-DYNA simulations to develop and analyze a new, cost effective, MASH TL-6 barrier. A literature review on computational methods to simulate sloshing behavior of a fluid inside a tank and a computational method for this model was established. Arbitrary Lagrangian-Eulerian was selected to analyze the fluid behavior inside the vehicle model, since this method is computationally inexpensive and re-mesh automatically.

To create the tank-trailer for the finite element analysis the components were extracted from a CAD model provided by LBT Inc., classified as critical, non-critical and complex components, and meshed in Hypermesh. The contacts and connections were done by comparing the LS-DYNA model with the actual tank trailer, by documenting how each component was attached. Also, a connection diagram was created to keep track of the contacts and constrains in the model. The element section was determined by measuring the thickness from each component in the CAD model and the element formulation for each component was selected depending on the type of element and the number of elements in the components.

Multiple fluid models were considered. It is recommended to further explore the fluid models in additional research phases to identify the most accurate and efficient fluid modeling technique which also provides the most accurate comparison with the existing physical test data. The material properties, and equations of state for each fluid is specified in the model to obtain a more accurate fluid behavior in the model simulation.

After the final version of the tank-trailer model is completed in a future study, it is anticipated that the model will be utilized by the international community to study multiple critical impact and explosive scenarios in the future.

References

1. Ross, H.E., Sicking, D.L., Zimmer, R.A., and Michie, J.D., *Recommended Procedures for the Safety Performance Evaluation of Highway Features*, National Cooperative Highway Research Program (NCHRP) Report No. 350, Transportation Research Board, Washington, D.C., 1993.

2. *Manual for Assessing Safety Hardware (MASH)*, Second Edition, American Association of State Highway and Transportation Officials (AASHTO), Washington, D.C., 2016.

3. Michie, J.D., Recommended Procedures for the Safety Performance Evaluation of Highway Appurtenances, National Cooperative Highway Research Program (NCHRP) Report 230, Transportation Research Board, Washington, D.C., March 1981.

4. Whitfield, D.L., Schmidt, J.D., Faller, R.K., Steelman, J., *Investigation of a Tractor-Tank Trailer Roadside Containment Barrier*, MATC Report No. 25-1121-005-004-11, MATC TRB RiP No. 91994-3, MwRSF Report No. TRP-03-404-18, Midwest Roadside Safety Facility, University of Nebraska-Lincoln, Lincoln, Nebraska, October 2018.

5. Rosenbaugh, S.K., Schmidt, J.D., Regier, E.M., Faller, R.K., *Development of the Manitoba Constrained-Width, Tall Wall Barrier*, TRP-03-356-16 Midwest Roadside Safety Facility, University of Nebraska-Lincoln, Lincoln, Nebraska, September 26, 2018.

6. Beason, W.L., and Hirsch, T.J., *Measurement of Heavy Vehicle Impact Forces and Inertia Properties*, Texas Transportation Institute, Texas A&M University, January 1989.

7. Ibrahim R.F., *Liquid Sloshing Dynamics Theory and Applications*, Cambridge University Press, 2006

8. Smith and Stojko, *The Application of Fluid Structure Interaction Techniques Within Finite Element Analyses Of Water-Filled Transport Flasks*.

9. Vesenjak et al., *Simulation of Fuel Sloshing – Comparative Study*.

10. Livermore Software Technology Corporation (LSTC). *LS-DYNA KEYWORD USER'S MANUAL VOLUME I*, Livermore, California, 2019.

11. Faller, R.K., Schmidt, J., Steelman, J.S., Whitfield, D., *Investigation and Development of a Test Level 6 Barrier, Phase I*, Final Report to the Mid-America Transportation Center, 2018.

12. Davidson, M.T., Chung, J.H., Teng, H., Han, Z., and Le, V., "Volume-Averaged Stress States for Idealized Granular Materials using Unbonded Discrete Spheres in LS-DYNA", Presented at the 10th European LS-DYNA Conference, Würzburg, Germany, 2015.

13. Jensen, A., Fraser, K., and Laird, G., "Improving the Precision of Discrete Element Simulations through Calibration Models", Presented at the 13th International LS-DYNA Users Conference.

https://www.predictiveengineering.com/sites/default/files/047_jensen_paper_improving_the_precision_of_discrete_element_simulations_through_calibration_models.pdf

14. *Aluminum in Commercial Vehicles*, European Aluminum Association, 2013. https://european-aluminium.eu/media/1295/aluminium-in-commercial-vehicle_en.pdf

Appendix A Tank-Trailer Description

Table A.1 Tank Components

Baffles, Bulkheads and Shell							
Part ID	**Component ID Geometry (Hypermesh)**	**Name**	**Element Type**	**Element Thickness**	**Element Size**	**Material ID**	**Section ID**
4	20	Baffle_1	Shell	6.3	19	6300002	6300012
8	503	Baffle_2	Shell	4.7	19	6300002	6300003
12	552	Baffle_3	Shell	4.7	19	6300002	6300003
20	17	Baffle_4	Shell	4.738	19	6300002	6300003
26	506	Baffle_5	Shell	6.3	19	6300002	6300002
31	508	Baffle_6	Shell	4.7	19	6300002	6300003
34	25	Bulkhead_1	Shell	6.35	19	6300002	6300002
37	514	Bulkhead_2	Shell	4.7	19	6300002	6300003
40	505	Bulkhead_3	Shell	4.7	19	6300002	6300003
43	2902	Bulkhead_4	Shell	4.7	19	6300002	6300003
46	555	Bulkhead_5	Shell	4.7	19	6300002	6300003
49	558	Bulkhead_6	Shell	4.7	19	6300002	6300003
52	559	Bulkhead_7	Shell	4.7	19	6300002	6300003
55	30	Bulkhead_8	Shell	6.35	19	6300002	6300008
6311713	1	Outer Shell	Shell	5.588	19	6300003	6300019
6311714	9		Shell	5.588	19	6300003	
6311734	2		Shell	5.588	19	6300003	
6311735	10		Shell	5.588	19	6300003	
6311736	4		Shell	5.588	19	6300003	

Table A.2 Fifth Wheel Components

Fifth Wheel							
Part ID	**Component ID Geometry (Hypermesh)**	**Name**	**Element Type**	**Element Thickness**	**Element Size**	**Material ID**	**Section ID**
62	75	Fifth Wheel Pin	Solid		6	6300005	45
63	71	Fifth-Wheel-1	Shell	7.9	12	6300005	6300006
64	72	Fifth-Wheel-2	Shell	4.8	12	6300005	6300007
65	74	Fifth-Wheel-3	Shell	7.9	12	6300005	6300006
	565		Shell	7.9	12		6300006
66	73	Fifth-Wheel-4	Shell	6.3	12	6300005	6300002
	564		Shell	6.3	12		
67	76	Fifth-Wheel-5	Shell	4.8	12	6300005	6300007
	566		Shell	4.8	12		

Table A.3 Chassis Components

Chassis Frame							
Part ID	**Component ID Geometry (Hypermesh)**	**Name**	**Element Type**	**Element Thickness**	**Element Size**	**Material ID**	**Section ID**
56	43	Beam_1	Shell	7.9	12	6300004	6300006
	56		Shell	7.9	12		
57	35	Beam_2	Shell	4.8	12	6300004	6300007
	516		Shell	4.8	12		
	529		Shell	4.8	12		
	532		Shell	4.8	12		
	534		Shell	4.8	12		
	535		Shell	4.8	12		
	536		Shell	4.8	12		
	537		Shell	4.8	12		
	538		Shell	4.8	12		
	542		Shell	4.8	12		

Table A.4 Chassis Components

Chassis Frame							
Part ID	**Component ID Geometry (Hypermesh)**	**Name**	**Element Type**	**Element Thickness**	**Element Size**	**Material ID**	**Section ID**
58	45	Beam_3	Shell	6.4	12	6300004	6300008
59	44	Beam_4	Shell	9.5	12	6300004	6300010
60	32	Bulk_Support	Shell	6.4	12	6300005	6300008
	33		Shell	6.4	12		
61	105	Fender	Shell	1.9	12	6300005	6300009
	305		Shell	1.9	12		
	365		Shell	1.9	12		
68	53	Rail	Shell	7.9	12	6300005	6300006
	54		Shell	7.9	12		6300006
69	46	Tank_Support 1	Shell	7.9	12	6300005	6300006
	47		Shell	7.9	12		6300006
	55		Shell	7.9	12		6300006
	57		Shell	7.9	12		6300006
70	50	Tank_Support 2	Shell	4.8	12	6300005	6300007
	52		Shell	4.8	12		
	525		Shell	4.8	12		
	526		Shell	4.8	12		
	527		Shell	4.8	12		
	549		Shell	4.8	12		
71	48	Tank_Support 3	Shell	9.5	12	6300005	6300010
	49		Shell	9.5	12		
72	51	Tank_tkg	Shell	5.6	12	6300005	6300011
73	18	TKE	Shell	6.3	12	6300005	6300002
	504		Shell	6.3	12		
	507		Shell	6.3	12		
	509		Shell	6.3	12		
	513		Shell	6.3	12		
	553		Shell	6.3	12		

Table A.5 Chassis Components

Chassis Frame							
Part ID	**Component ID Geometry (Hypermesh)**	**Name**	**Element Type**	**Element Thickness**	**Element Size**	**Material ID**	**Section ID**
74	373	TKE1	Shell	4.7	12	6300005	6300003
75	41	TKG1	Shell	6.4	12	6300005	6300008
	522		Shell	6.4	12		
76	58	TKG2	Shell	6 side, 7.9 middle	12	6300005	6300014
	68		Shell	6.2 side, 7.9 middle	12		
	560		Shell	6.2 side, 7.9 middle	12		
	561		Shell	6.2 side, 7.9 middle	12		
	562		Shell	6.2 side, 7.9 middle	12		
77	69	TKG3	Shell	5.6	12	6300005	6300011
	70		Shell	5.6	12		
	563		Shell	5.6	12		
78	64	TKG4	Shell	6.4	12	6300005	6300008
	556		Shell	6.4	12		
79	352	TKG5	Shell	4.7	12	6300006	6300003
	1917		Shell	4.7	12		
80	355	TKG6	Shell	6.4	12	6300005	6300008
	356		Shell	6.4	12		
81	359	TKG7	Shell	3.2	12	6300005	6300015
	360		Shell	3.2	12		
	362		Shell	3.2	12		
82	42	TKG8	Shell	9.5	12	6300006	6300010
	524		Shell	9.5	12		
83	354	TKG11	Shell	3.2	12	6300005	6300015
	1918		Shell	3.2	12		
	1919		Shell	3.2	12		
	3236		Shell	3.2	12		
84	2990	TKG13	Shell	4.7	12	6300005	6300003
85	114	TKG14	Shell	4.7	12	6300005	6300003
	2996		Shell	4.7	12		
86	115	TKG15	Shell	6.3	12	6300005	6300002

Appendix B Connection Diagram

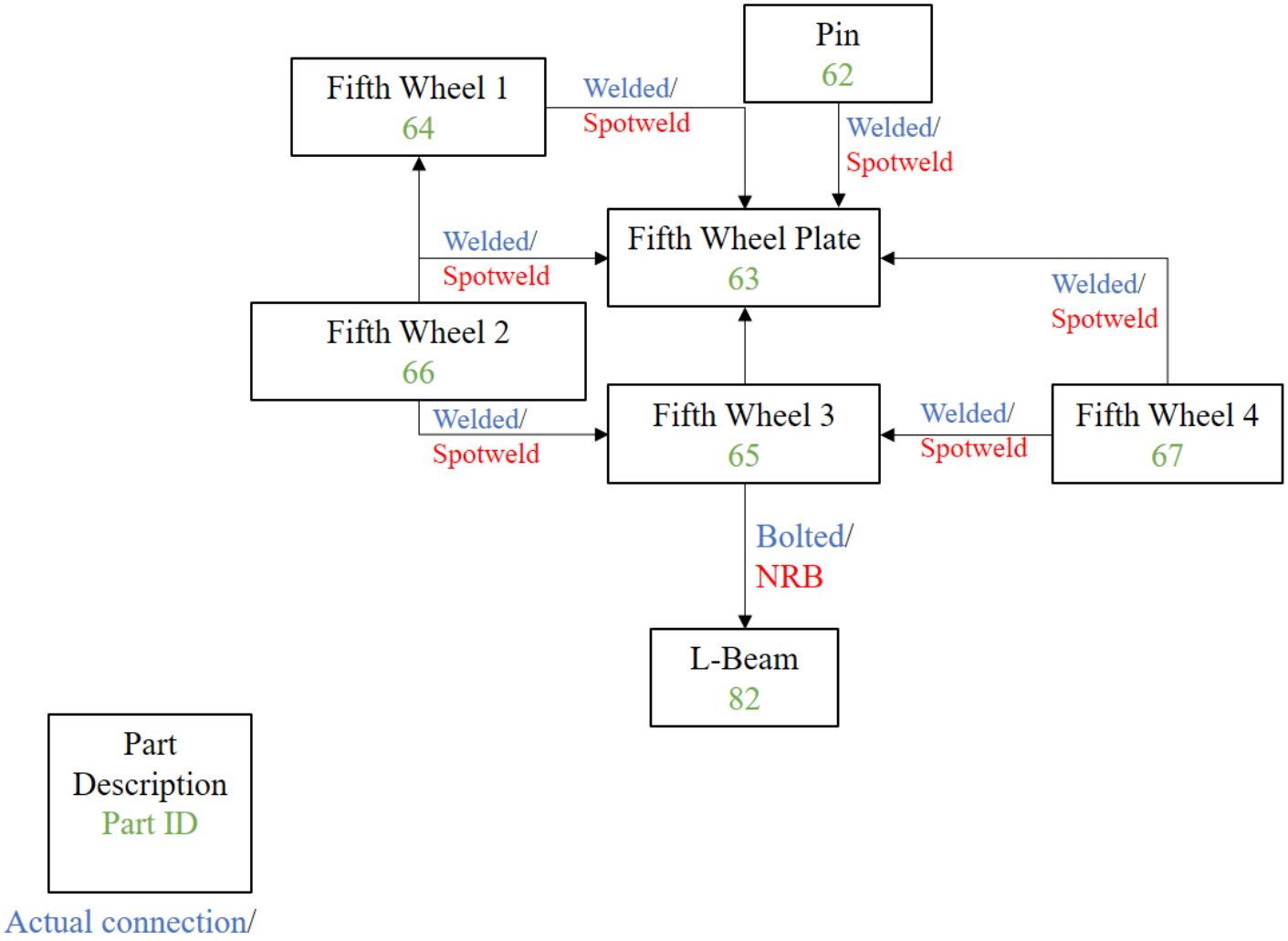

Figure B.1 Fifth Wheel Connection Diagram

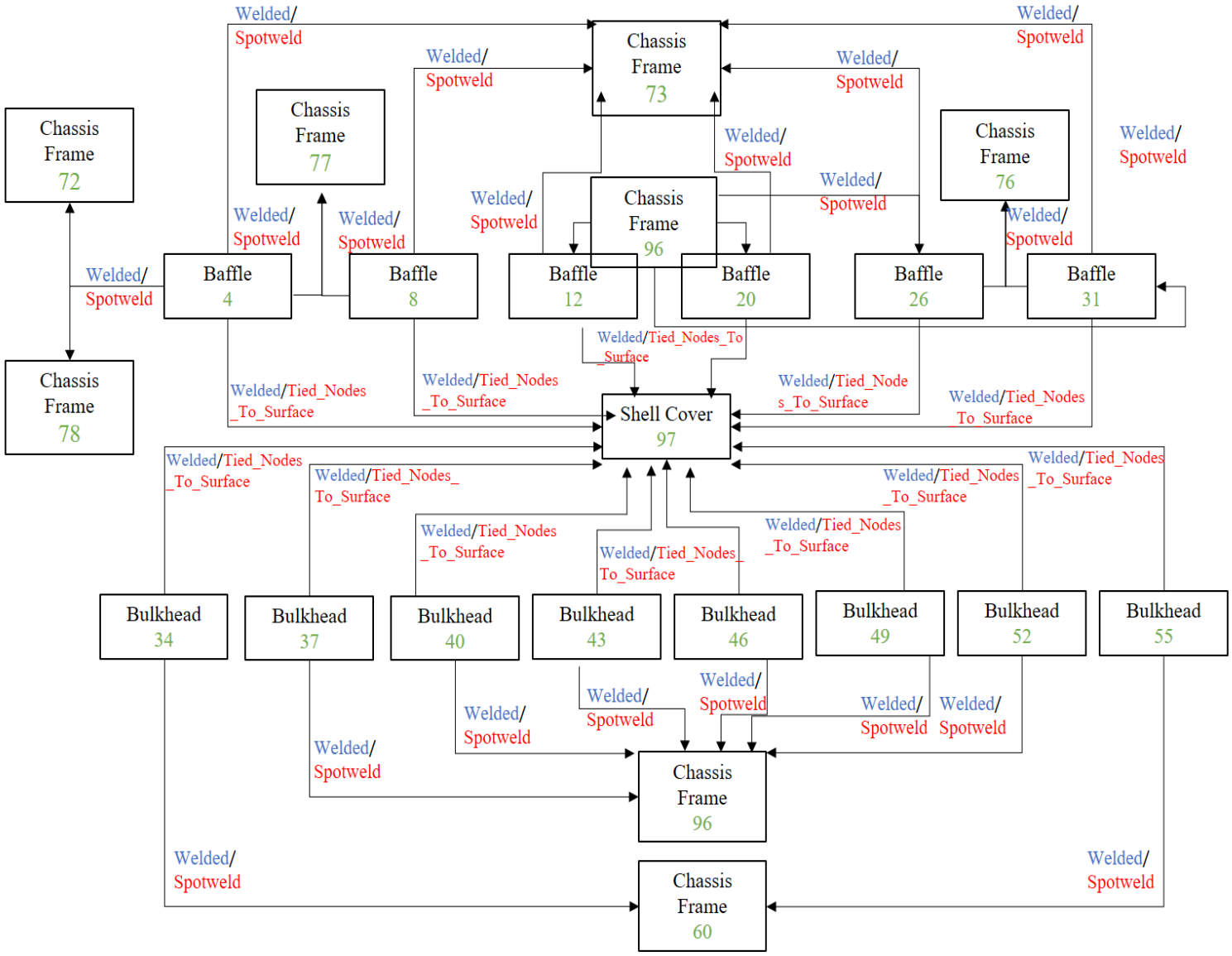

Figure B.2 Tank, Baffle and Bulkhead Connection Diagram

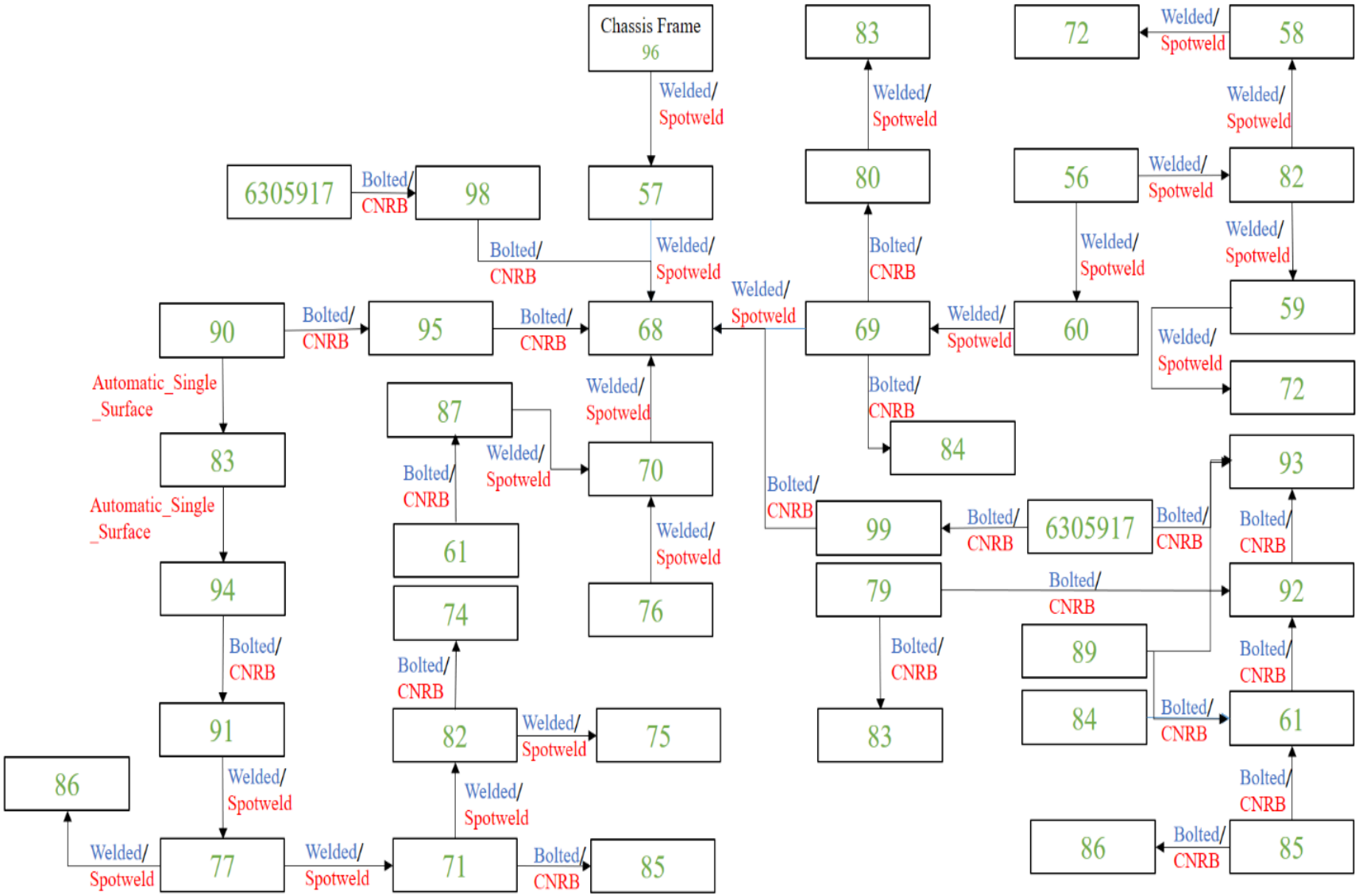

Figure B.3 Chassis Frame Connection Diagram